Experimental Neurology 358 (2022) 114220

Contents lists available at ScienceDirect

Experimental Neurology

journal homepage: www.elsevier.com/locate/yexnr

Research paper

Aberrant perineuronal nets alter spinal circuits, impair motor function, and increase plasticity

J. Sánchez-Ventura [a], C. Canal [a], J. Hidalgo [a], C. Penas [a], X. Navarro [a], A. Torres-Espin [b], K. Fouad [c], E. Udina [a,*]

[a] Institute of Neuroscience, Department Cell Biology, Physiology and Immunology, Universitat Autònoma de Barcelona, and Centro de Investigación Biomédica en Red sobre Enfermedades Neurodegenerativas (CIBERNED), Bellaterra, Spain
[b] Weill Institute for Neuroscience, Brain and Spinal Injury Center (BASIC), Department of Neurological Surgery, University of California San Francisco, San Francisco, CA, USA
[c] Neuroscience and Mental Health Institute, Department of Physical Therapy, Faculty of Rehabilitative Medicine, University of Alberta, Edmonton, AB, Canada

ARTICLE INFO

Keywords:
Perineuronal nets
Link protein 1
Plasticity
Locomotion
Spinal cord injury

ABSTRACT

Perineuronal nets (PNNs) are a specialized extracellular matrix that have been extensively studied in the brain. Cortical PNNs are implicated in synaptic stabilization, plasticity inhibition, neuroprotection, and ionic buffering. However, the role of spinal PNNs, mainly found around motoneurons, is still unclear. Thus, the goal of this study is to elucidate the role of spinal PNNs on motor function and plasticity in both intact and spinal cord injured mice. We used transgenic mice lacking the cartilage link protein 1 (*Crtl1* KO mice), which is implicated in PNN assembly. *Crtl1* KO mice showed disorganized PNNs with an altered proportion of their components in both motor cortex and spinal cord. Behavioral and electrophysiological tests revealed motor impairments and hyperexcitability of spinal reflexes in *Crtl1* KO compared to WT mice. These functional outcomes were accompanied by an increase in excitatory synapses around spinal motoneurons. Moreover, following spinal lesions of the corticospinal tract, *Crtl1* KO mice showed increased contralateral sprouting compared to WT mice. Altogether, the lack of *Crtl1* generates aberrant PNNs that alter excitatory synapses and change the physiological properties of motoneurons, overall altering spinal circuits and producing motor impairment. This disorganization generates a permissive scenario for contralateral axons to sprout after injury.

1. Introduction

Perineuronal nets (PNNs) are a dynamic extracellular matrix that surround neurons in the central nervous system (CNS) and play a key role in synaptic stabilization and plasticity inhibition (reviewed in Wang and Fawcett, 2012). They are composed of chondroitin sulfate proteoglycans (CSPGs), hyaluronan and proteins such as tenascin-R, link proteins and Semaphorin 3A (Dick et al., 2013; Kwok et al., 2011). PNN formation is activity dependent and occurs at late postnatal stage, specifically at the end of the 'critical period' for plasticity which coincides with the maturation of neural circuits and the decline of neural plasticity (Berardi et al., 2000; Pizzorusso, 2002; Dityatev et al., 2007). In fact, the enzymatic breakdown of PNNs by chondroitinase (ChABC) reopens the plasticity window, demonstrating the implication of PNNs in this process (Pizzorusso, 2002). Among all PNN components, the cartilage link protein 1 (Crtl1) is crucial in PNN formation since its expression closely follows the assembly of PNNs (Carulli et al., 2010). In vitro, its absence prevents PNN formation around PNN-bearing cells (Kwok et al., 2010). In vivo, its genetic deletion confers increased levels of plasticity in the adult visual cortex and Purkinje cell terminals and also promotes regeneration into the denervated cuneate nucleus (Carulli et al., 2010; Foscarin et al., 2011).

In the mature CNS, the role of PNNs in regulating plasticity-stability processes has been extensively studied in the brain, demonstrated in the visual cortex (Pizzorusso, 2002), amygdala (Nadine et al., 2009), medial prefrontal cortex (Slaker et al., 2015), and the cerebellum (Carulli et al., 2020). Other functions have been attributed to cortical PNNs, such as ionic buffering (Brückner et al., 1993), neuroprotection (Suttkus et al., 2014), and synaptic refinement (Frischknecht et al., 2009). In contrast, little is known about PNNs' function within the spinal cord even though they surround 80% of α-motoneurons (MNs) and many spinal interneurons (Irvine and Kwok, 2018).

* Corresponding author.
E-mail address: esther.udina@uab.cat (E. Udina).

https://doi.org/10.1016/j.expneurol.2022.114220
Received 9 June 2022; Received in revised form 24 August 2022; Accepted 28 August 2022
Available online 3 September 2022

Interestingly, spinal PNNs thickness is modulated by neuronal activity in the opposite direction of cortical PNNs, since activity reduces brain PNNs but increases spinal ones (Smith et al., 2015). Thus, decreased spinal motoneurons activity below a SCI reduces the thickness of their PNNs. This reduction is reversed by physical rehabilitation (Sánchez-Ventura et al., 2020), and depends on increased synaptic activity (Arbat-Plana et al., 2015; Smith et al., 2015). It is interesting to note that application of ChABC at the injury site in SCI models, degrades CSPGs secreted by the fibro-glial scar, and attenuates the growth limiting properties of CSPGs (Barritt et al., 2006; Massey et al., 2006; Vavrek et al., 2007). However, the plasticity achieved by ChABC only establishes meaningful connections and translates into functional recovery when combined with rehabilitative motor training (García-Alías et al., 2009; Tom et al., 2009; Wang et al., 2011), to facilitate the formation and stabilization of functional connections. This synaptic stabilization is comparable to that found at the end of the developmental critical period in which PNNs participate.

Despite sound and promising evidence, most studies highlight the potential of ChABC to boost plasticity in the spinal cord without properly evaluating the importance of modulating PNNs. Thus, the current study aims to describe the role of spinal PNNs on motor function by using transgenic mice lacking the Hyaluronan and Proteoglycan Link protein 1 (Crtl1/HAPLN1) gene, which encodes the cartilage link protein1 (Crtl 1), a key element triggering PNN formation (Carulli et al., 2010). In previous research, *Crtl1* KO mice were used to study PNNs' role in the cerebellum and brain (Carulli et al., 2010; Foscarin et al., 2011). Within the present study, our goal was to study the functional importance of PNNs in the motor system using behavioral, electrophysiological, and histological analysis in *Crtl1* KO mice. Elucidating PNN function in the spinal cord will improve our understanding of its role in fine-tuning synaptic plasticity and stability.

2. Materials and methods

2.1. Experimental design

Transgenic mice (*Crtl1* KO) used in this study were provided by Dr. Pizzorusso (Carulli et al., 2010) and maintained in the Animal Service of the Universitat Autònoma de Barcelona (UAB).

Their generation and phenotype are described by *Czipri* et al (Czipri et al., 2003). In brief, *Crlt1* KO mice lack for the cartilage link protein 1, encoded by the Crtl1/HAPLN1 gene, which is required for the proper assembly of PNNs (Fig. 1). These *Crtl1* KO mice are rescue transgenic mice, in which Crtl1is expressed under the control of the type II collagen cartilage-specific promoter and enhancer, resulting in Crtl1 expression in cartilage but depletion in all tissues including the CNS (Carulli et al., 2010). This specific overexpression is produced to avoid skeletal malformations incompatible with life (Suppl. Fig. 1). They are maintained in a C57BL6/J genetic background.

Ninety-six female and male adult (8–12 weeks of age) *Crlt1* KO mice and their WT littermates were used. A total of 62 mice were used for characterization and 34 for evaluating the role of link protein 1 in sprouting after SCI. From the 62 mice used for characterization, 20 were randomly chosen for histological analysis. Since no sex differences were detected (Suppl. Fig. 2), data from both sexes was pooled. All experiments were blinded to genotype during behavioral testing and histological analysis.

The experimental procedures were approved by UAB Experimental Ethical Committee (CEAAH) and conducted following the animal welfare guidelines 2010/63/EC of the European Communities Council Directive. Mice were housed in groups, at 22 °C (± 2 °C), kept on a 12:12 light/dark cycle and received water and food ad libitum.

2.2. Genotyping

The genotype of mice (Table 1) was determined using mouse tail genomic DNA and 3 specific sets primers by PCR (Table 2).

2.3. Functional assessment

Animals were handled for 3 days and habituated for 15 min in the behavioral room before each test.

2.3.1. Open field test

Open field testing was used to measure general locomotor activity (Seibenhener and Wooten, 2015). Mice were individually placed into a white methacrylate box (56 × 36,5 × 31 cm) and allowed to explore for 5 min. Their exploratory behavior was recorded for automated assessment. The total distance, and the average speed traveled were analyzed from recorded footage with Ethovision XT version 11.5 (Noldus) software, whereas the number of rearings was annotated during the test session.

2.3.2. Novel object recognition test (NORT)

NORT was performed in the Open field arena. Mice were habituated during 3 consecutive days (10 min) to the arena. The familiarization phase started on the 4th day. During this session, two identical objects (A1 and A2) were placed in the middle of the arena and mice explored them for 10 min. Two hours after familiarization, short-term memory was tested by placing mice back into the arena for 10 min, where one of the familiar objects was replaced by a novel object (B). To test long-term memory, animals were put back in the box 24 h after the familiarization phase, to explore the familiar object A and a second novel object C (10 min). The time spent with each object – when an animal sniffed or touched it – was measured. Finally, a discrimination index (DI) was calculated as the difference between the time spent with the novel or familiar objects divided by the total time spent with the two objects at 2, 5 and 10 min cumulatively. A higher DI reflects greater memory consolidation for the familiar object (Bevins and Besheer, 2006). All objects had similar sizes but different shapes and colors. Between trials, ethanol was applied to the objects to avoid the use of odor cues.

2.3.3. Pole test

The pole test is used to evaluate coordination and balance (Ogawa et al., 1985). A pole (50 cm high, 1 cm in diameter) was vertically placed on a soft platform, which contains the nesting material of the animal home cage to motive the mouse to climb down. Following a brief period (30 s) of ground exploration, each mouse was placed on the top of the pole and the time required to turn head down (T-turn) and descend the pole (T-descend) was measured. A maximum of 120 s was allowed to complete the task. If the mouse fell from the top of the pole, this trial was discarded. Each mouse underwent 3 consecutive trials.

2.3.4. Adapted rotarod

Standard rotarod tests evaluate motor function and coordination (Shiotsuki et al., 2010). To also assess motor learning, the test was repeated during 4 consecutive days at a constant velocity of 10 rpm (Shiotsuki et al., 2010). The day before training sessions, mice were habituated to stay on the stopped rotarod for 3 min. This habituation protocol was repeated every test day for 1 min, just before the training session started. In each session, mice were placed on the rotarod and the latency to fall was measured. Immediately after falling, mice were placed back on the drum up to 5 times. A fall was overlooked when the animal endured on the drum for 180 s. Finally, the total fall latencies of each day were summed and compared between the 4 days and groups. The habituation and the training session were performed at the same time of the day.

2.3.5. DigiGait and maximal velocity assessment

The maximal velocity that animals could reach was evaluated on a treadmill. Locomotion kinematics was evaluated through the DigiGait system (Mouse Specifics, Boston, MA) in which animals were placed

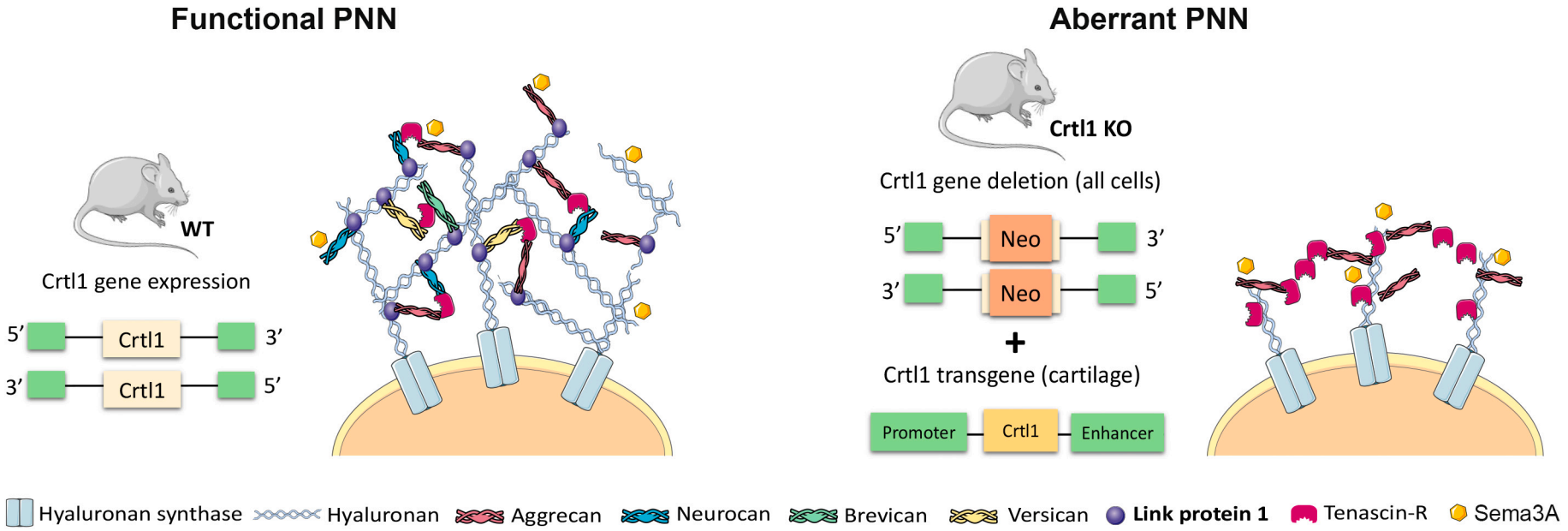

Fig. 1. Schematic diagram illustrating the genetic differences between the *Crtl1* KO and WT mice and their corresponding PNN structure. WT mice present highly organized and functional PNN. These nets are anchored to neurons by the enzyme hyaluronan synthase, which produces a hyaluronan polymer chain. This chain provides a scaffold for the binding of different types of CSPGs of the lectican family (aggrecan, neurocan, brevican and versican), whose interaction is stabilized by the link protein 1. Finally, the tenascin-R interconnects the different chains of CSPGs, generating a complex structure. The Sema3A protein can bind to the PNN's structure. In the *Crtl1* KO mice, the expression of the *Crtl1* gene is disrupted by the addition of a Neomycin vector in all cells. In the cartilage, there are normal levels of Crtl1 expression given that these mice overexpress the Crtl1 gene under the control of a cartilage-specific promoter. Crtl1 KO mice present disorganized PNNs due to the lack of the stabilizer link protein 1. Sema3A: semaphorin 3A; WT: wild type; KO: knock-out; PNN: perineuronal nets; *Crtl1*: cartilage link protein 1; Neo: neomycin.

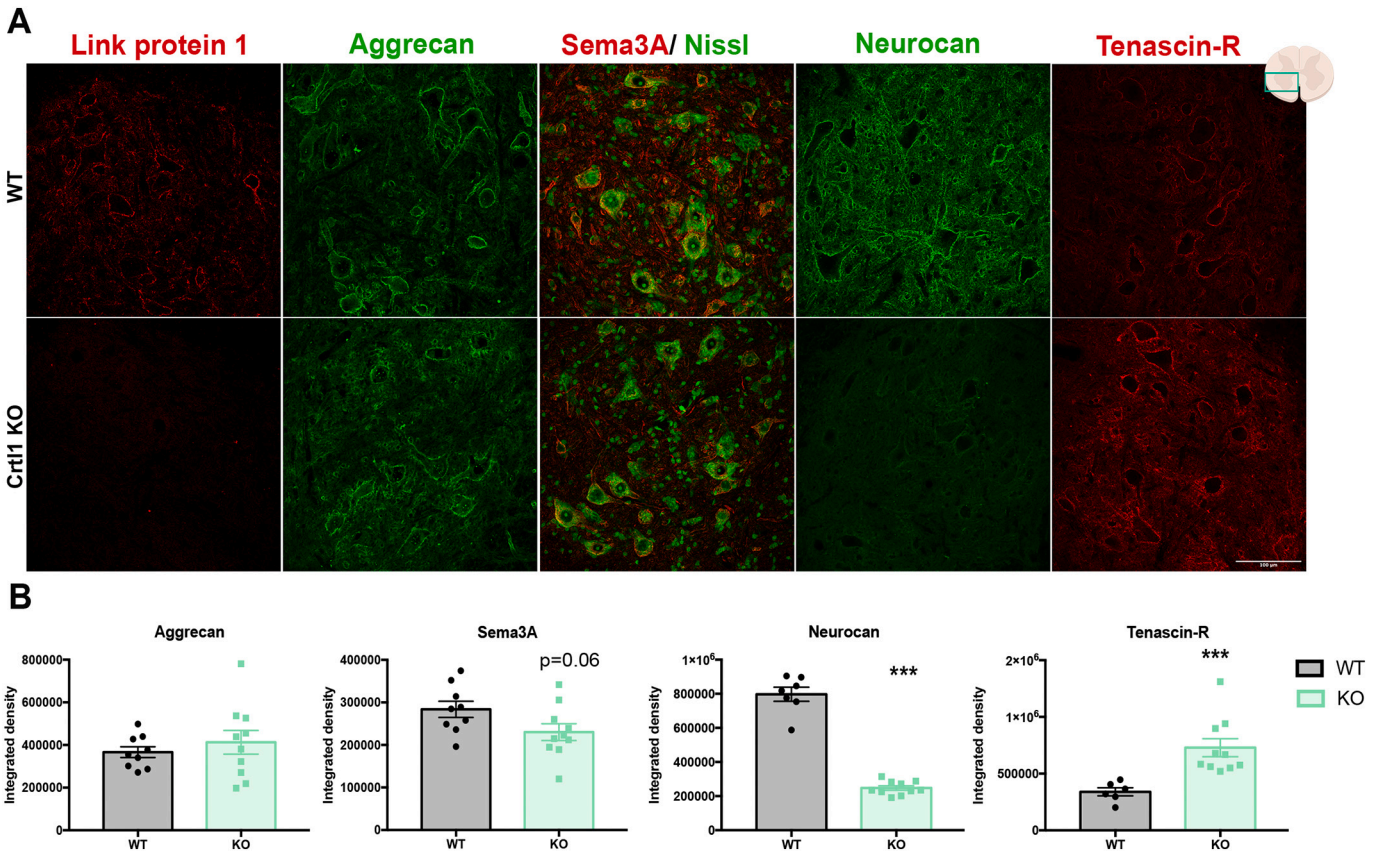

Fig. 2. The lack of link protein 1 generates PNNs with altered proportion of their components in the lumbar spinal cord. A. Maximal projection of confocal images showing the expression of different components of PNNs around lumbar MNs: link protein 1 (red), aggrecan (green), semaphorin 3A (red) around Nissl positive-cells (green), neurocan (green) and tenascin-R (red). B. Quantification of the immunolabeling of PNN components. $N_{total} = 19$ mice. Bar graphs are representing the mean values ± SEM. Scale bar: 100 μm. $^{**}p < 0.01$, $^{***}p < 0.001$ by Weltch *t*-test. Crtl1: cartilage link protein 1; WT: wild type; KO: knock-out. (For interpretation of the references to colour in this figure legend, the reader is referred to the web version of this article.)

Table 1
Genotypes generated.

	Neomycin	Crtl1	MC59
WT (*Crtl1* +/+)	−	+	−
Heterozygous (*Crtl1* +/− Crtl1-Tg +/0 or *Crtl1* +/−)	+	+	+/−
KO (*Crtl1* −/− *Crtl1*-Tg +/0)	+	−	+

Table 2
Primer sequences and PCR conditions.

Gene	F/R	Sequence	PCR conditions
Crtl1	F	5' TAATGACCTTTCCTGTCTCTCC 3'	94 °C for 2 min, 35× (94 °C for 15 s, 60,5 °C for 30s, 72 °C for 5 min) and 72 °C for 5 min.
	R	5' CCCAAAACCCGTAGTTCC 3′	
Neomycin	F	5' CTTGGGTGGAGAGGCTATTC 3'	95 °C for 3 min, 35× (95 °C for 30s, 60 °C for 30s, 72 °C for 45 s) and 72 °C for 2 min.
	R	5' AGGTGAGATGACAGGAGATC 3'	
Crtl1 cartilage (MC59)	F	5' CCTTTCAGACAGCTACACTCC 3'	94 °C for 2 min, 30 x (94 °C for 30s, 59 °C for 30s, 72 °C for 1 min) and 72 °C for 5 min.
	R	5' AAACACTCGACCTTGATAGCC 3'	

onto the treadmill belt at 20 cm/s, based on previous results of our laboratory (Mancuso et al., 2011). Only those *Crtl1* KO mice that could reach that velocity were included in the DigiGait analysis. A high-speed video camera (150 frames/s) located below the transparent belt was used to monitor around 10–12 strides/animal. Two trials were given to each animal to obtain an appropriate video for analysis, which was considered when mice walked straight ahead at a constant velocity. Then, each video was digitized, and the area of the paw was calculated with the DigiGait software. Mistakes of the imaging in which the paw area was not correctly detected were manually corrected. Parameters such as the percentage of duration of the stride phases, the ratio between the stance and the swing phase, the paw area at the stance phase and the dA/dT_{max} and dA/dT_{min} were evaluated.

2.3.6. Grip strength

The limb strength of all mice was determined using the grip strength test (Meyer et al., 1979). For three days, mice were placed on a grid strength apparatus so they could grab a small grid with their fore and both fore and hindlimbs. Afterwards, mice were slowly pulled away from the grid until they release it. The maximal peak force was measured using a sensor connected to the grip strength apparatus. Each day, five trials of 15 s were performed and averaged. All the values were normalized using the body weight of each mouse.

2.3.7. Electrophysiological tests

To evaluate the state of spinal reflexes, electrophysiological tests were performed under anesthesia (ketamine 90 mg/kg and xylazine 10 mg/kg) since it has negligible effects on electrophysiological recordings (Ho and Waite, 2002).

For stretch reflex measurements, the sciatic nerve was stimulated by delivering a single electrical pulse of 0.02 ms at supramaximal intensity (Grass S88) by a monopolar needle inserted in the sciatic notch. The compound muscle action potential (CMAP) of the plantar muscle was recorded using a monopolar needle inserted in that muscle. In this recording, the maximal baseline to peak amplitude of the M wave (M_{max}: direct muscle response), initial and final M wave latencies, and the maximum amplitude of the H wave (H_{max}: monosynaptic reflex) were measured. Finally, the H_{max}/M_{max} was calculated as an index of the excitability of the Ia afferent synapses on spinal MNs (Thompson et al., 1992). While M wave values were obtained with supramaximal stimulations, the H_{max} was elicited after progressively increasing the intensity of the electrical stimulation until reaching the maximal amplitude of the H wave. The depression profile of the H wave or rate-dependent depression (RDD) was performed following the protocol previously described (Sánchez-Ventura et al., 2020).

Regarding the withdrawal reflex, the ipsilateral polysynaptic reflex was elicited by stimulating the sciatic nerve with a pulse of 0.1 ms at a supramaximal intensity and the potentials were recorded at the ipsilateral tibialis anterior muscle. The contralateral polysynaptic reflex was elicited by stimulating the left tibial nerve at the ankle and recorded at the right tibialis anterior muscle. The maximum amplitude, and the area under the curve (Root Mean Square; RMS) of the third component (C3) were evaluated, which is conveyed by C fibers and found in latencies between 18 and 55 ms (Valero-Cabré et al., 2004).

For motor units' evaluation, the mean amplitude of single motor unit activation potentials (SMUA) was assessed. From a subthreshold intensity, the sciatic nerve was stimulated with pulses that progressively increased their intensity and recorded in the plantar and tibialis anterior muscle. Increments higher than 50 μV were considered as indicative of the recruitment of an additional motor unit. Finally, the mean amplitude of individual motor units was calculated as the average of consistent increases.

All recorded potentials were amplified and visualized on a digital oscilloscope (Tektronix 450S). LabChart Reader software was used for the analysis.

2.4. Spinal cord injury

To determine the potential of the corticospinal axons to sprout and grow after injury, a unilateral dorsal hemisection at the C4 level (HxC4) was performed. Before the injury, the following experimental groups were randomly generated: WT sham ($n = 6$); WT+ HxC4 ($n = 12$); *Crtl1* KO sham ($n = 10$); *Crtl1* KO + HxC4 (n = 6).

For the surgical procedure, mice were anesthetized using an intraperitoneal injection (i.p.) of ketamine (90 mg/kg) and xylazine (10 mg/kg) in saline solution. After skin and muscle incision, a laminectomy of segment C3-C4 was performed to expose the spinal cord. Then, a unilateral dorsal hemisection of the left C4 spinal cord was done, using small scissors, to a depth of 1.0 mm to completely sever the dorsolateral corticospinal tract. To ensure that the lesion was complete, the scissors were passed through the dorsal part of the spinal cord three times. After surgery, animals received 1 ml of saline solution subcutaneously. For pain management, subcutaneous injections of buprenorphine (0.1 mg/kg) were administered. Mice were kept on a 38 °C heating pad during the surgical procedure and until they were fully awake.

2.5. Biotinylated dextran amine tracing

To anterogradely label the axons of the corticospinal tract (CST), 1,5 μl of the neuronal tracer biotinylated dextran amine (BDA; 10,000 MV; 10% in PB; Thermo Fisher) were injected in the left motor cortex. Briefly, 7 days after injury, mice were deeply anesthetized with ketamine/xylazine (see above) and placed in a stereotaxic device to perform the craniotomy and the injection of the tracer. The injection was set up in three points of the left motor cortex (ipsilateral to SCI): −1 mm lateral to the midline, at 0.5 mm, −0.5 mm and − 1 mm from Bregma and at a depth of 0.7 mm ventral to the dura. A 10 μl Hamilton syringe fitted with a 33 G needle was used. Each injection delivered 0.5 μl of the tracer at a velocity rate of 0.25 μl/min and the syringe was left at the site of injection for 3 min before removal. Two weeks after injection, animals were euthanized.

2.6. Histological evaluation

Mice were euthanized (pentobarbital; *ip:* 200 mg/kg) and transcardially perfused with 4% paraformaldehyde (PFA) in 0.1 M phosphate buffer (PB). Spinal cords, brains and tibialis anterior muscles were harvested. Spinal cords and brains were post-fixed in 4% PFA over 2 h and overnight (ON), respectively. Afterwards, both tissues were cryoprotected in 30% sucrose solution in PB at 4 °C until tissue sank, while tibialis anterior muscles were directly cryopreserved in that solution.

For the *Crtl1* KO histological analysis, lumbar spinal cords (L4-L5), motor cortices (Bregma 0.98 to 1.94) and tibialis anterior muscles were transversally cut on a cryostat (20 μm thick) and collected onto gelatin-coated glass slides. To study PNN components (L4-L5 spinal segment and motor cortex), synaptic markers (L4-L5 spinal segment) and muscle fibers, tissue sections were permeabilized with Phosphate Buffer saline Triton 0.3% (PBST 0.3%) except for the KCC2 marker, which was permeabilized with PBST 0.3%-Bovine Serum Albumin 3%. Then, nonspecific interactions were blocked with 10% Normal Donkey Serum for 1 h at room temperature (RT). Afterwards, sections were incubated ON at 4 °C with primary antibodies (Table 3). After washes, immunoreactive sites were revealed using species-specific secondary antibodies (1:200; 2 h RT; Table 3). For Neurocan and Semaphorin 3A (Sema3A) markers, the signal was amplified by streptavidin (1:200) and biotin tyramide (1:60; TSA Biotin System; Perkin Elmer NEL700001KT) for 1 h and 3 min, respectively. Finally, sections were coverslipped using Fluoromount-G medium (Southern Biotech).

For sprouting evaluation, the C1 level of the spinal cord was cross-sectioned (20 μm), whereas the rest of the cervical spinal cord was longitudinally cut (25 μm). Both types of sections were immunolabeled to detect the BDA tracer. For BDA detection, sections were initially washed with TBS-Tween 0.1 and then, endogenous peroxidases were blocked for 10 min. Next, we incubated the streptavidin-HRP (1:200) for 1 h at RT. After several washes, the signal was amplified incubating the biotin tyramide (1:50) for 7 min and visualized with Alexa Fluor 488-streptavidin (1:200) after 1 h at RT.

2.6.1. Image analysis

To analyze PNN components and synaptic markers, images were taken from 4 spinal cord (L4-L5) or brain sections (motor cortex) using a confocal laser-scanning microscope (around 30 steps, z-step size of 0.5 μm, Leica TCS SP5) at 40× for each mouse. To quantify PNNs and synaptic changes, a minimum of 30 MNs (located within the ventral horn and presenting an area $> 350\ \mu m^2$ (Friese et al., 2009)) were measured for each animal. PNN analysis was performed as described before (Sánchez-Ventura et al., 2020). In brief, the maximal projection of the z-stacks was performed and then, the background was corrected. Then, a band of 4 μm around the cell body of MNs was delimited to measure the integrated density of that region. For synaptic measurements, VGlut1 (vesicular glutamate transporter 1) and VGAT (vesicular GABA transporter) + synaptic boutons presented in a band of 4 μm around the selected MN were measured by integrated density. Synaptic competition between proprioceptive afferents and C-boutons (Jiang et al., 2016) was assessed by counting the number of VGlut1 positive synaptic boutons and C-boutons positive dots presented in the whole photograph.

For spinal MN analysis, slides corresponding to L4-L5 spinal cord sections separated 200 μm each were stained using ChAT (choline acetyltransferase) and MMP9 (matrix metalloproteinase 9) antibodies. The number of lumbar MN was determined by counting the number of

Table 3
List of primary and secondary antibodies used in the histological analysis.

Primary antibodies				Secondary antibodies		
Antibody	Dilution	Host	Reference	Antibody	Host	Reference
Aggrecan (Cat301)	1:100	Mouse	MAB5284- Sigma Aldrich	Alexa Fluor 488	Donkey x Mouse	A21202 - Invitrogen
Link protein 1	1:100	Goat	AF2608-SP, R&D systems	Alexa 594	Donkey x Goat	A11058- Invitrogen
Sema3A	1:400	Goat	OASG06564 – Aviva Systems biology	Streptavidin- Cys3		43–4315- Zimed
Neurocan	1:50	Sheep	AF5800- R&D systems	Strepatividin 488		S11223- Invitrogen
Tenascin- R	1:200	Goat	AF3865- R&D systems	Alexa Fluor 594	Donkey x Goat	A11058- Invitrogen
VGlut1	1:300	Guinea Pig	AB5905- Millipore	Cys 3	Donkey x Guinea Pig	706–165-148- Jackson
VGAT	1:1000	Rabbit	131,002- Synaptic systems	Alexa Fluor 488	Donkey x Rabbit	A21206-Invitrogen
KCC2	1:400	Rabbit	07–432- Millipore	Alexa Fluor 594	Donkey x Rabbit	A21207- Invitrogen
ChAT	1:50	Goat	AB144P, Millipore	Alexa Fluor 488	Donkey x Goat	A 11055-Invitrogen
MMP9	1:200	Rabbit	ab38898, Abcam	Cys 5	Donkey x Rabbit	711–175-152- Jackson
Collagen IV	1:100	Mouse	M3F7, Hybridoma Bank	Alexa Fluor 594	Donkey x Mouse	A21203 - Invitrogen

ChAT+ cells located in lamina IX of grey matter (bilaterally). The percentage of MMP9+ cells was then calculated from the total of ChAT+ neurons. To quantify KCC2 staining at the dorsal horn, confocal images were obtained at 40× and the integrated density of the whole immunoreactivity was measured. For the VGlut1 marker, images were captured at 20× and the integrated density of immunoreactivity was measured in a region of interest (ROI) of 0.175 mm^2. After background correction, the threshold was defined for all the microphotographs of the same marker.

The estimated number of muscle fibers found in the tibialis anterior muscle was calculated counting the number of fibers – delimitated by the collagen IV staining – in 5 regions of 0,8043 μm^2 (captured at 20×) in a single muscle section. Then, the total area of the muscle slice (captured at 4×) was used to estimate the total number of muscle fibers. Two tibialis anterior muscle sections were used in each animal and obtained results were averaged.

To evaluate the sprouting of contralateral axons induced by the cervical injury, we first estimated the number of traced axons of the CST. Images from C1 sections containing the BDA tracer were taken at 40× and the total number of traced axons of the CST was counted in two different sections and averaged. Longitudinal sections were captured at 10× and then, the count of CST collaterals was performed at C3-C6 over

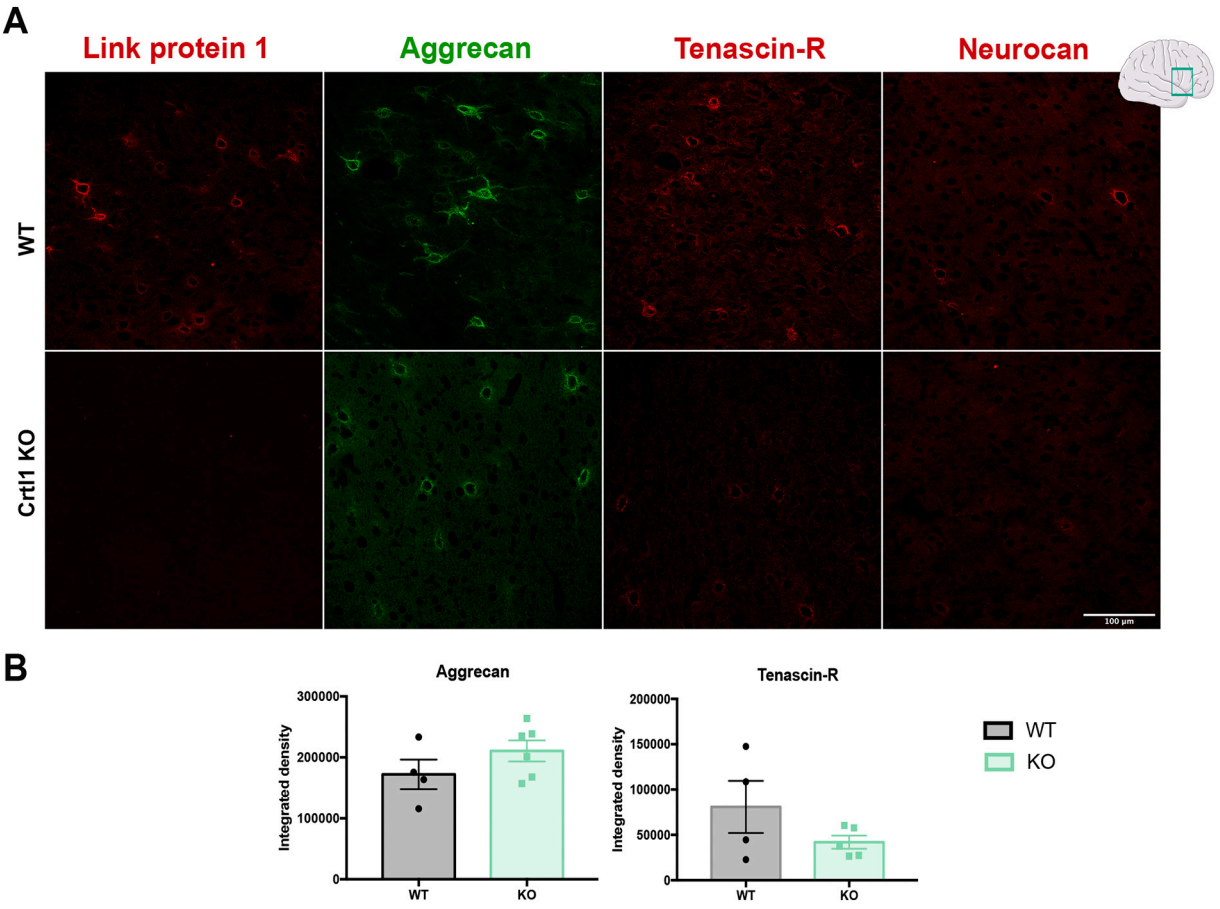

Fig. 3. Characterization of PNN components in the motor cortex of the *Crtl1* KO mice. A. Confocal images in which cortical PNNs are stained against the link protein 1 (red), aggrecan (green), tenascin-R (red) and neurocan (red). B. Quantification of the immunolabeling of aggrecan and tenascin-R around neurons. Neurocan quantification is not shown due to the little staining found in the WT group. $N_{total} = 10$ mice. Bar graphs are representing the mean values ± SEM. Scale bar: 100 µm. Significant different were neither found by unpaired *t*-test (aggrecan) nor Weltch t-test (tenascin-R). Crtl1: cartilage link protein 1; WT: wild type; KO: knock-out. (For interpretation of the references to colour in this figure legend, the reader is referred to the web version of this article.)

14 sections (separated by 50 μm each), and thus, evaluating a total extension of 700 μm of the spinal cord. Finally, the number of traced axons at C1 was used to normalize the sprouting in each animal.

Image analysis was performed by Fiji software.

2.7. Statistical analysis

Data is analyzed using GraphPad Prism 7 software and shown as mean ± standard error of the mean (SEM). Differences were considered significant when $p < 0.05$. Shapiro-Wilk test confirmed a normal distribution of each response variable/group. Thus, functional results were analyzed by Student's *t*-test (unpaired), since variables presented equal variance except for the adapted rotarod, pole test, DigiGait analysis, grip strength and NORT which were analyzed by two-way ANOVA repeated measures followed by pairwise post-hoc contrast with Bonferroni adjustment of *p* values. Histological results were analyzed by Student's t-test except for the MN distribution and the VGlut1 analysis at the dorsal horn that were evaluated by two-way ANOVA with same post-hoc as above. Considering Student's t-test for histological analysis, those variables that did not present equal variance (PNN analysis) were evaluated by Weltch t-test.

3. Results

3.1. The lack of link protein 1 altered PNN composition in the spinal cord

We first corroborated the absence of link protein 1 in the central nervous system of *Crtl1* KO mice. Immunofluorescence of the link protein 1 was neither detected in the lumbar spinal cord (Fig. 2A) nor the motor cortex (Fig. 3A). Since link protein 1 is implicated in the assembly of PNNs, we next studied PNN components of the *Crtl1* KO mice by immunolabeling aggrecan, neurocan, Sema3A and tenascin-R in lumbar spinal cord samples (Fig. 2A). No significant differences in the intensity of aggrecan labeling between WT and *Crtl1* KO mice were observed (Fig. 2B). Nevertheless, the aggrecan distribution in *Crtl1* KO mice seemed more diffuse than in WT animals, suggesting a less dense PNN. Moreover, aggrecan was only distributed around the soma, with almost no staining around dendrites (Fig. 2A), consistent with the motor cortex (Fig. 3A, B). In addition, Sema3A staining at lumbar levels was reduced although not significantly in *Crtl1* KO compared to WT mice ($p = 0.06$; Fig. 2A, B). Finally, *Crtl1* KO mice showed a marked reduction of neurocan ($p < 0.001$) and increased tenascin-R ($p < 0.001$) in the spinal cord (Fig. 2B). Notably, the tenascin-R increase was also visible across the grey matter parenchyma (Fig. 2A). In contrast, the expression of tenascin-R moderately decreased in cortical PNNs of *Crtl1* KO mice, albeit not significantly (Fig. 3B). Neurocan was not quantified in the motor cortex due to the faint staining observed in the WT group (Fig. 3A).

3.2. Crtl1 KO mice presented reduced body weight and hypoactivity

Crtl1 KO mice of both sexes had significantly less weight compared to WT mice ($p < 0.01$ in males and $p < 0.001$ in females; Fig. 4A). Evaluation of general overground locomotion (Open field arena) revealed that *Crtl1* KO mice were hypoactive since their travel distance ($p < 0.001$), locomotor velocity ($p < 0.001$) and time locomoting ($p < 0.001$) were reduced compared to WT mice. Similarly, *Crtl1* KO mice showed reduced explorative behavior, with fewer rearings ($p < 0.001$) (Fig. 4B).

3.3. Animals lacking link protein 1 displayed impaired locomotion, motor coordination and abnormal gait performance

The observed hypoactivity prompted us to investigate whether it was caused by motor deficits. We addressed this using some complementary functional motor tests that allow us to evaluate motor coordination, locomotion, and motor learning. Animals lacking link protein 1 could not reach the maximum velocity values obtained by WT mice on a treadmill ($p < 0.001$, Fig. 5A). Adapted rotarod gives us information about motor coordination and motor learning. We found that *Crtl1* KO mice could not stay as long on the rotarod as WT mice (significantly

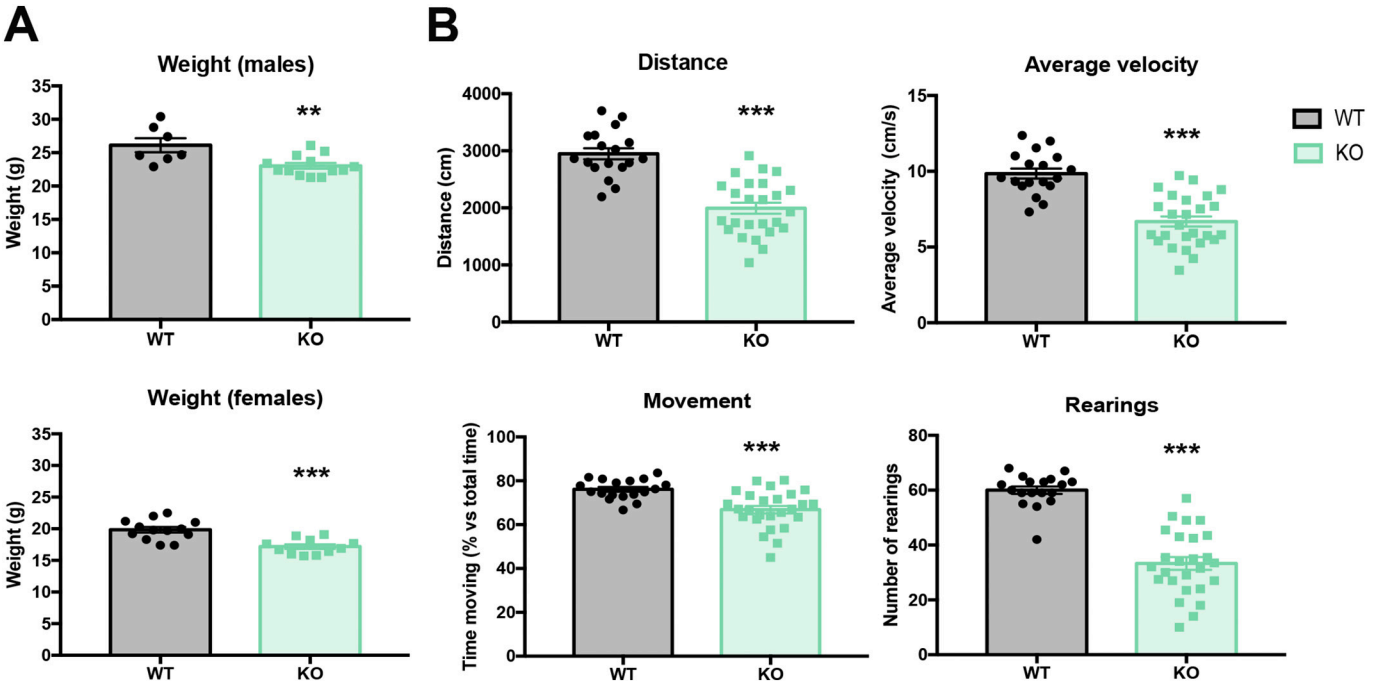

Fig. 4. *Crtl1* KO mice present reduced weight and hypoactivity assessed by Open Field test. A. Males and females *Crtl1* KO mice presented reduced body weight. B. Open Field test revealed that *Crtl1* KO present hypoactivity observed in the total distance traveled, average velocity, percentage of time in movement and number of rearing performed in 5 min. $N_{total} = 44$ mice. Bar graphs are representing the mean values ± SEM. $^{**}p < 0.01$, $^{***}p < 0.001$ by unpaired *t*-test. WT: wild type; KO: knock-out.

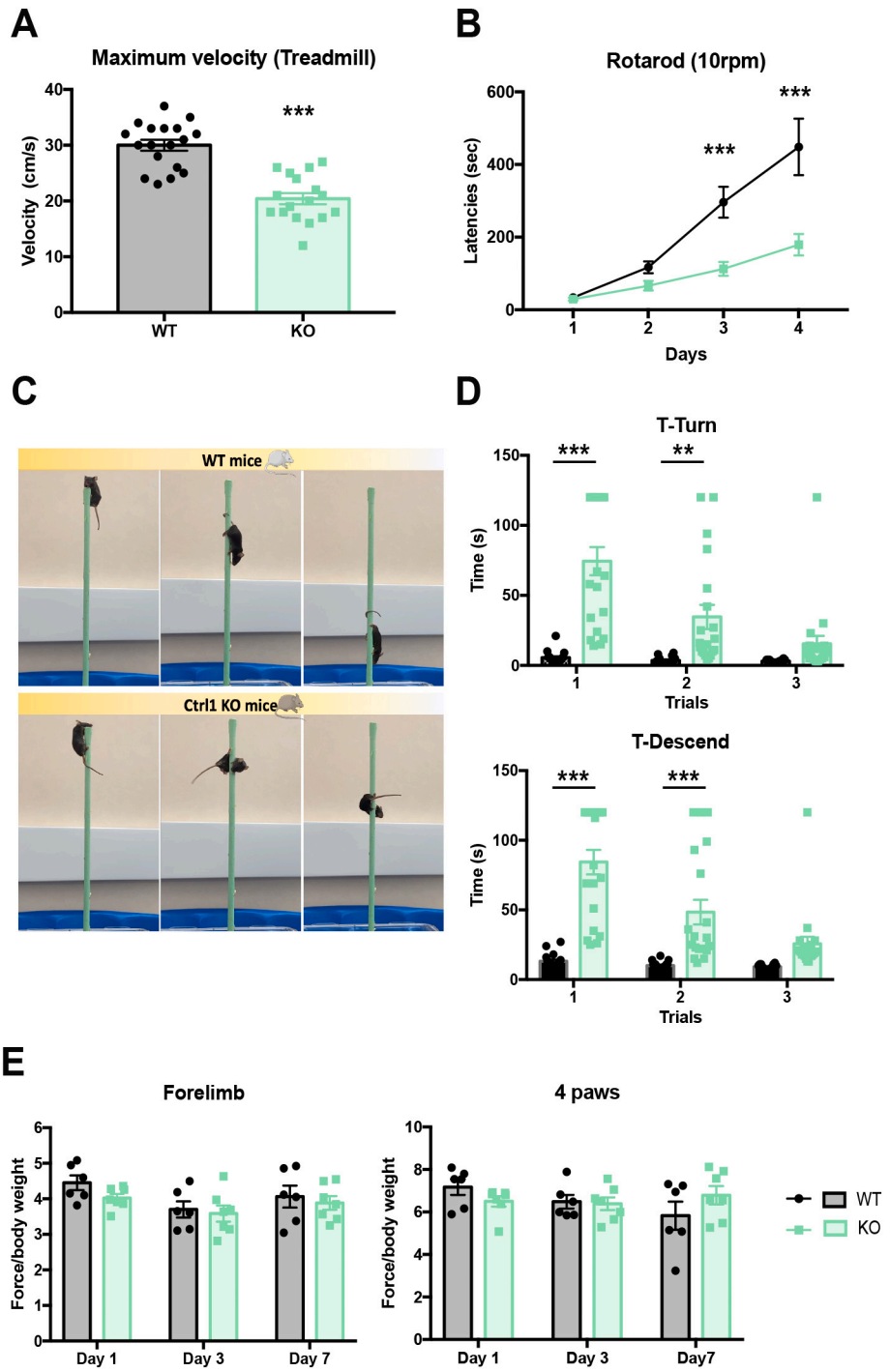

Fig. 5. *Crtl1* KO mice displayed altered locomotor activity, coordination, and motor learning. A. Evaluation of the maximum velocity reached by *Crtl1* KO and WT mice on a treadmill. $N_{total} = 35$ mice. B. Quantification of the daily amount of time (latency) of *Crtl1* KO and WT mice sustained performance in the adapted rotarod during four consecutive sessions. $N_{total} = 30$ mice. C. Photographs representing the two possibilities to climb down the pole: turning 180° (WT mice) or climbing down in a horizontal position (*Crtl1* KO mice). D. Representation of the time required for the *Crtl1* KO and WT mice to turn down (T-turn) and descend the pole (T-descend) in three consecutive trials. $N_{total} = 38$ mice. E. Assessment of the grip strength of the forelimb and the 4 paws of *Crtl1* KO and WT mice for three days. $N_{total} = 14$ mice. Data are representing the mean values ± SEM. ***p < 0.001 by unpaired t-test for the maximum velocity and **p < 0.01, ***p < 0.001 by two-way ANOVA (*Adapted rotarod*: time $F_{3,123} = 53.72$, p < 0.001; group $F_{1,41} = 19.76$, p < 0.001; interaction $F_{3,123} = 12.66$, p < 0.001; *T-turn*: time $F_{2,72} = 24.63$, p < 0.001; group $F_{1,36} = 27.34$, p < 0.001; interaction $F_{2,72} = 20.82$, p < 0.001; *T-descend*: time $F_{2,72} = 27.79$, p < 0.001; group $F_{1,36} = 39.67$, p < 0.001; interaction $F_{2,72} = 20.93$, p < 0.001) followed by post hoc test with Bonferroni correction. Crtl1: cartilage link protein 1; WT: wild type; KO: knock-out.

different in the last two days of testing ($p < 0.001$; Fig. 5B)). Performance of WT mice on the rotarod also improved over four consecutive days whereas *Crtl1* KO mice exhibited limited improvement (interaction effect over time: p < 0.001; day 1 vs 2 WT and KO $p > 0.05$; day 2 vs 3 WT p < 0.001, KO p > 0.05; day 3 vs 4 WT $p < 0.01$, KO p > 0.05). During the pole test (also for motor coordination), WT mice turned 180° to orient themselves downward and descend the pole, whereas almost all *Crtl1* KO mice failed to turn 180° and descended in a horizontal position (Fig. 5C). The analysis showed that *Crtl1* KO mice spend more time turning down (T-turn; 1st trial p < 0.001 and 2nd trial $p < 0.01$) and descending the pole (T-descend) (both trials p < 0.001) compared to WT mice (Fig. 5D). In contrast, Crtl1 KO mice did not present alterations in the limb strength evaluated by the grip strength test compared to WT (Fig. 5E; p > 0.05).

Considering the marked motor discoordination observed, DigiGait was used for walking pattern analysis in both genotypes. Percentages of the stride phases in the *Crtl1* KO mice were altered in both forelimb ($p < 0.001$ in brake and $p < 0.05$ in propulsion phase) and hindlimb (p < 0.001 in swing and propulsion phase) compared to WT mice. Consequently, these alterations decreased the stance/swing ratio in the hindlimb of *Crtl1* KO mice compared to WT mice (p < 0.001). The plantar placement of the hindlimb of *Crtl1* KO mice was also reduced, represented as a smaller paw area compared to WT mice. dA/dT_{min} and $_{max}$ refer to the maximal rate of change of paw area in contact with the treadmill belt during the propulsion and braking phase, respectively. Thus, dA/dT_{min} shows how rapidly the animal can propel itself into the

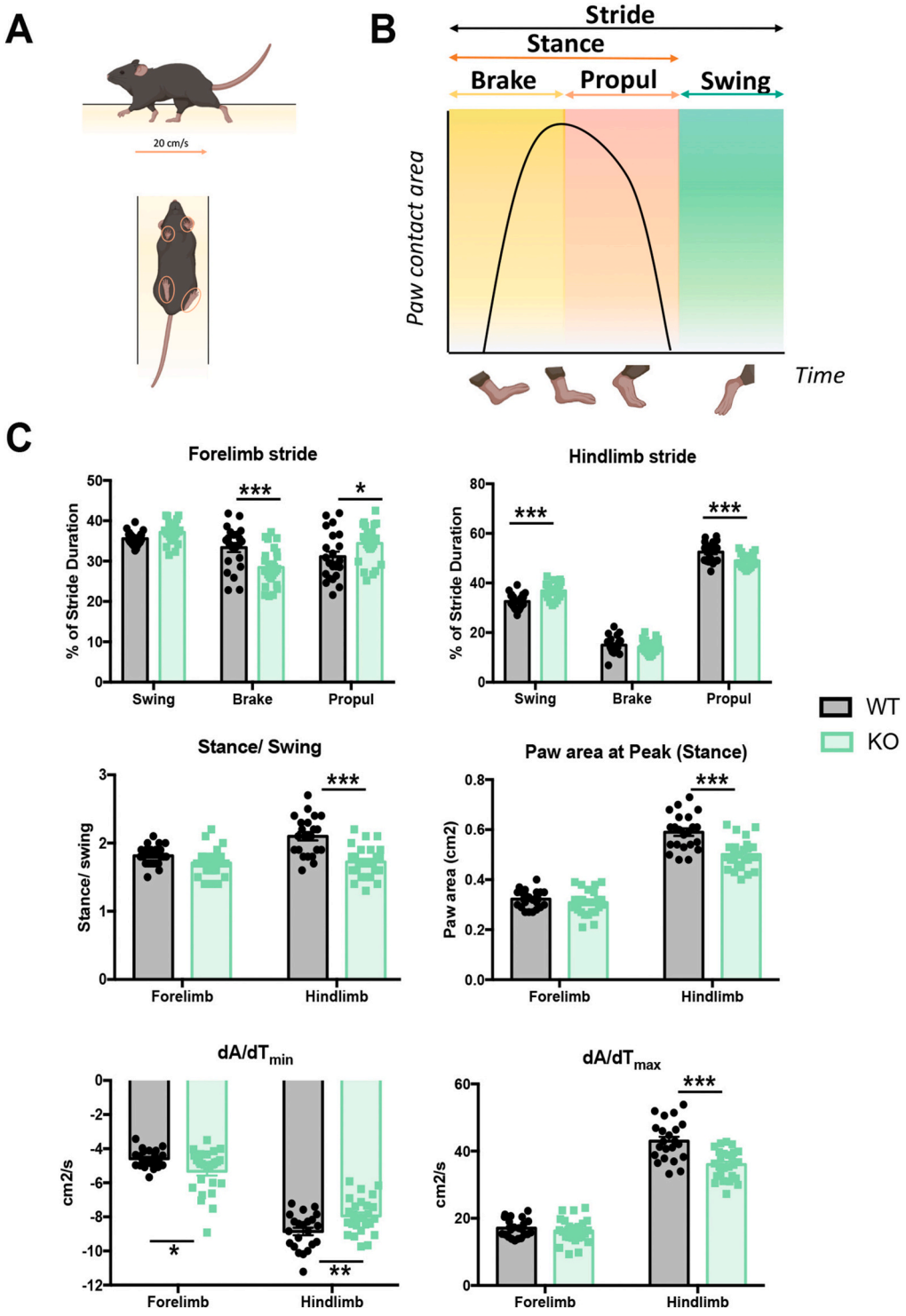

Fig. 6. ***Crtl1* KO mice showed altered gait performance**. A. Scheme of the experimental procedure in which mice run on a treadmill bell at 20 cm/s and their paws (marked in orange) are analyzed. B. Schematic representation of the different phases of the stride. The stride is divided into two parts: the swing and the stance phase, the latter is further divided into the brake and propulsion phase. The swing phase coincides when there is no paw contact with the treadmill belt. The brake phase includes from the initial paw contact to the maximum paw contact and the propulsion phase includes from the maximum paw contact to just before the swing phase starts. C. Gait analysis: representation of the % of duration of the different phases of the stride in both fore and hindlimb, the Stance/swing ratio, the maximum paw area at the peak, and the rate of change of paw area contact with the treadmill belt (dA/dT). $N_{total} = 23$ mice. Bar graphs are representing the mean values ± SEM. *$p < 0.05$, **$p < 0.01$, ***$p < 0.001$ by two-way ANOVA (*Forelimb stride*: time $F_{2,92} = 13.12$, $p < 0.001$; group $F_{1,46} = 1.476$, $p = 0.231$; interaction $F_{2,92} = 8.03$, $p = 0.006$; *Hindlimb stride*: time $F_{2,92} = 1096$, $p < 0.001$; group $F_{1,46} = 3.138e\text{-}010$, $p > 0.99$; interaction $F_{2,92} = 13.27$, $p < 0.001$; *Stance/swing*: time $F_{1,46} = 17.96$, $p < 0.001$; group $F_{1,46} = 20.74$, $p < 0.001$; interaction $F_{1,46} = 14.48$, $p = 0.004$; *Paw area at peak*: time $F_{1,46} = 1239$; $p < 0.001$; group $F_{1,46} = 12.73$, $p = 0.009$; interaction $F_{1,46} = 32.52$, $p < 0.001$; dA/dT_{min}: time $F_{1,46} = 378.2$, $p < 0.001$; group $F_{1,46} = 0.147$, $p = 0.703$; interaction $F_{1,46} = 21.77$, $p < 0.001$; dA/dT_{max}: time $F_{1,46} = 1599$; $p < 0.001$; group $F_{1,46} = 12.78$, $p < 0.001$; interaction $F_{1,46} = 29.06$, $p < 0.001$) followed by post hoc test with Bonferroni correction. WT: wild type; KO: knock-out; Propul: propulsion.

next step, while dA/dt $_{max}$ shows how quickly the limb is loaded during the initial period of stance (Fig. 6B). Our data demonstrated that *Crtl1* KO mice presented altered values in both parameters compared to WT mice (Fig. 6C) in the forelimb ($p < 0.05$ in dA/dT min analysis) and hindlimb ($p < 0.01$ in the dA/dTmin and $p < 0.001$ in the dA/dT max).

Since PNNs have already been described to have a role in memory consolidation (Nadine et al., 2009; Fawcett et al., 2019), we corroborated the altered functionality of PNNs in our *Crtl1* KO mice by evaluating short- and long-term memory using the NORT (Suppl. Fig. 3A). *Crtl1* KO mice had a greater ability to recognize a new object in the short-term memory test ($p < 0.05$ at 2 min) but showed impaired long-term memory consolidation ($p < 0.01$ at 2 min; Suppl. Fig. 3B).

3.4. *Crtl1 KO mice presented increased excitability of spinal reflexes*

Electrophysiological tests were used to assess if the motor

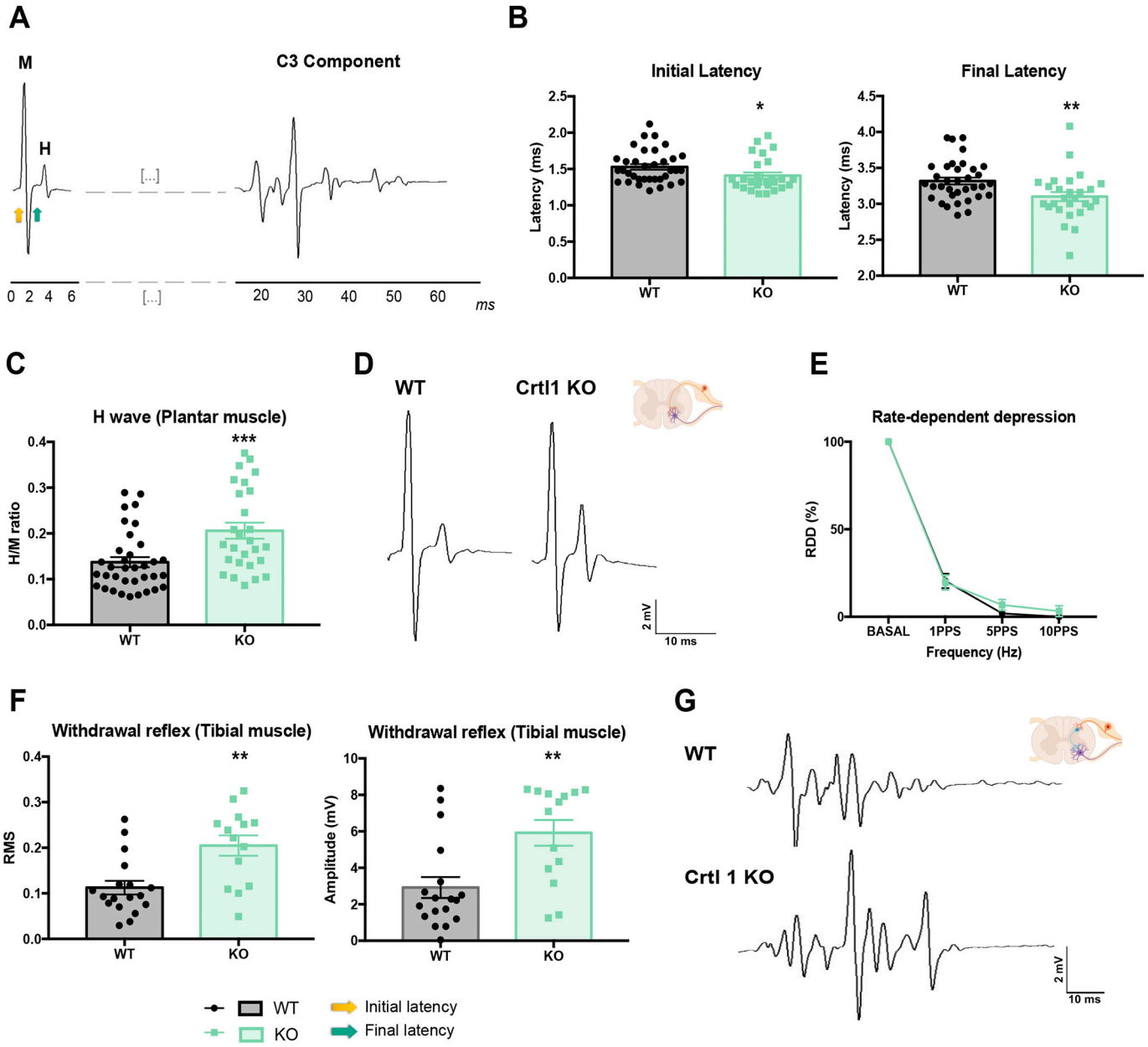

Fig. 7. ***Crtl1* KO mice presented increased excitability of spinal circuits observed in both monosynaptic and polysynaptic spinal reflexes.** A. Representative image of the recordings studied. At the left side of the image, it is represented the different components of the compound muscle action potential (CMAP): the M and the H wave. These waves are measured to evaluate the stretch reflex (monosynaptic). $N_{total} = 62$ mice. The colored arrows represent the onset (yellow) and final (green) latencies of the M wave. At the right side of the image, the C3 component of the withdrawal reflex is represented, whose maximum amplitude and the area under the curve are analyzed. B. Quantification of the onset and final latencies of the M wave studied in the plantar muscle. C. H/M ratio studied in the plantar muscle. D. Representative electromyographs showing the CMAP in the WT and *Crtl1* KO mice. E. Depression profile of the H wave after consecutive stimulations at different frequencies. F. Evaluation of the area under the curve (RMS) and maximum amplitude of the C3 component of the withdrawal reflex, recorded at the ipsilateral tibialis anterior muscle. $N_{total} = 32$ mice. G. Representative electromyographs showing the C3 component of the withdrawal reflex in the WT and Crtl1 KO mice. Data are representing the mean values ± SEM. *$p < 0.05$, **$p < 0.01$, ***$p < 0.001$ by unpaired t-test. No significant differences were found in the depression of the H wave (RDD) analyzed by two-way ANOVA (time $F_{3,180} = 926.8$, $p < 0.001$; group $F_{1,60} = 0.514$, $p = 0.476$; interaction $F_{3,180} = 0.781$, $p = 0.506$) followed by a post hoc test with Bonferroni correction. Crtl1: cartilage link protein 1; WT: wild type; KO: knock-out. (For interpretation of the references to colour in this figure legend, the reader is referred to the web version of this article.)

impairments observed in the *Crtl1* KO mice were linked to alteration in spinal networks. Stimulation of the sciatic nerve elicited a M wave with reduced initial ($p < 0.05$) and final latency ($p < 0.01$) in *Crtl1* KO mice compared to WT mice (Fig. 7B). Regarding the stretch reflex (or H-reflex), *Crtl1* KO mice exhibited an increased H/M ratio compared to WT mice ($p < 0.001$). Since the stretch reflex is a monosynaptic reflex in which only proprioceptive (Ia) afferences and MNs participate, this hyperexcitability could be caused by an alteration of local circuitry between MNs and Ia afferences, or inhibitory descending pathways. These inhibitory descending pathways regulate the amount of presynaptic inhibition that Ia afferents received and thus, indirectly adjust the stretch reflex (Faist et al., 1994). To elucidate the origin of this hyperexcitability, we studied the state of inhibitory descending pathways by evaluating the RDD of the H wave. Given that *Crtl1* KO and WT mice presented a similar pattern of depression, we assumed that these descending pathways were unaffected (Fig. 7E). Thus, the hyperexcitability observed in the H/M ratio may be caused by a change at the local MN circuitry. Next, the polysynaptic withdrawal reflex was evoked at the tibialis anterior muscle and assessed by C3 component evaluation (Fig. 7G). Increased hyperreflexia in both the ipsilateral ($p < 0.01$; Fig. 7F) and contralateral side (Suppl. Fig. 4) was observed in transgenic animals compared to WT group, indicating a general hyperexcitability of the spinal reflex circuits in *Crtl1* KO mice.

3.5. Mice with aberrant PNNs exhibited a general increase in excitatory but not inhibitory synapses

To complement the functional analysis and further study spinal circuits, we evaluated the composition of spinal synapses in *Crtl1* KO mice. We found that lumbar MNs from *Crtl1* KO mice received a greater number of excitatory (VGlut1), but not inhibitory (VGAT) inputs compared to WT mice (Fig. 8A, B; $p < 0.001$ in the VGlut1 analysis). In contrast, however, KCC2, whose reduction is a hallmark of hyperexcitability (Boulenguez et al., 2010), was unaltered in the *Crtl1* KO group (Fig. 8A, B). Therefore, the hyperexcitability observed in the electrophysiological test could be caused by an increase in excitatory inputs. Consistent with this, the increased expression of VGlut1 was also notable in the dorsal horn of *Crtl1* KO mice ($p < 0.001$). Of note, *Crtl1* KO mice showed increased KCC2 staining in the dorsal horn ($p < 0.001$; Suppl. Fig. 5).

Given that motoneurons from *Crtl1* KO mice presented a high number of proprioceptive inputs (VGlut1), we wondered whether this increase could impact on the number of C-boutons (marked with ChAT) received (Fig. 8C). We observed an increase of both VGlut1 and C-boutons in MNs from *Crtl1* KO compared to WT mice ($p < 0.001$; Fig. 8D), suggesting a general increase of excitatory synapses around MNs with aberrant PNNs.

3.6. Altered PNNs modified the lumbar motoneuron size and motor unit properties

We discarded that the motor impairment was caused by MN loss as we did not find differences in the number of ChAT+ cells between groups (Fig. 9A). However, we noticed a reduction in the mean area of motoneuron soma of *Crtl1* KO compared to WT animals ($p < 0.001$; Fig. 9B). This reduction could be mediated by a general reduction in the somatic area of all motoneurons or due to a decrease in the percentage of bigger neurons. Thus, we generated a distribution graph representing the number of MN found depending on their size. Fig. 9C revealed a significant increase in the number of small MNs (between 300 and 450 μm) and a reduction in large MNs (between 650 and 750 μm) in *Crtl1* KO compared to WT mice ($p < 0.01$, $p < 0.001$). To confirm whether this change in soma size is related to MN physiological properties, we stained MNs with anti-MMP9, a marker of MN from fast motor units (Kaplan et al., 2014) (Fig. 9E). We found a reduction in the percentage of MMP9+/ChAT+ cells in *Crtl1* KO compared to the WT group ($p < 0.05$; Fig. 9D). Altogether, these results suggested that Crtl1 KO presents a shift in the lumbar MN pool composition, leading to an increase in slow motor units and a decrease in fast ones.

To evaluate the functional repercussion of this shift, motor unit recruitment and muscle properties were assessed (Suppl. Fig. 6). Crtl1 KO mice presented a higher mean amplitude of their motor units (SMUA) compared to WT mice in both plantar ($p < 0.01$) and tibialis anterior muscle ($p < 0.001$). At the muscle level, Crtl1 KO mice showed a reduced number of muscle fibers in the tibialis anterior muscle ($p < 0.05$), as well as a reduction in the weight of the muscle studied ($p < 0.05$ in absolute values and $p < 0.001$ related to the body weight).

3.7. Crtl1 KO mice displayed increased corticospinal sprouting after spinal cord injury

To further evaluate the impact of cartilage link protein 1 on motor function, we next studied the corticospinal tract (CST) and its potential to sprout after SCI (Suppl. Fig. 7A). No significant differences were found in the number of fibers traced CST fibers between groups measured at C1 spinal level (Suppl. Fig. 7B, C). After unilateral dorsal hemisection at the C4 level, the contralateral CST of *Crtl1* KO mice showed increased sprouting of spared axons below the injury level compared to WT mice ($p < 0.05$). Once contralateral axons reached the denervated side of the cord, a high density of small axons was found near the midline rather than observing long sprouts crossing the grey matter. No significant differences were observed in the percentage of contralateral projections between uninjured groups (Suppl. Fig. 7D, E).

4. Discussion

Although most spinal MNs are wrapped by PNNs, their functional role and the impact of their degradation remain largely unexplored. However, ChABC application on the spinal cord has been used extensively in experimental models to promote axonal growth post-SCI (Bradbury et al., 2002; Fawcett, 2015). Thus, our goal was to assess the role of spinal PNNs on motor spinal networks.

4.1. Crtl1 KO mice show aberrant PNNs with an altered proportion of their components

To study the role of PNNs, we used *Crtl1* KO mice as they lack the *Crtl1/HAPLN1* gene, which encodes the cartilage link protein 1, crucial for PNNs formation during development. Once PNNs are formed, link proteins stabilize the interaction between CSPGs to the hyaluronan backbone in the net structure (Spicer et al., 2003). In the present work, we have found that aggrecan can still accumulate around the neuronal soma despite the lack of link protein 1, generating aberrant PNNs in these *Crtl1* KO mice. Similar findings were reported by *Carulli* et al in the brain (Carulli et al., 2010). The presence of aggrecan allowed tenascin-R to attach to the remaining CSPGs and hence, contribute to this aberrant PNN deposition. In contrast, neurocan was almost absent in PNNs of *Crtl1* KO mice. These altered PNNs were also found in neurons of the motor cortex. Thus, *Crtl1* KO mice presented aberrant PNNs with disorganized morphology and altered proportion of their components.

4.2. Aberrant PNNs increase the excitability of spinal circuits

PNNs are highly organized structures that play a crucial role in stabilizing mature synapses initially formed during development. In our study, *Crtl1* KO mice showed an increased number of excitatory, but not inhibitory synapses around lumbar MNs. One of the mechanisms that allow PNNs to restrict synapse formation is the expression of Sema3A (Vo et al., 2013). In our KO mice, we found a slight reduction of Sema3A in PNNs, which could partially facilitate synaptogenesis. The reduced levels of neurocan could also lead to this increased synaptic content since it contributes to neuronal outgrowth inhibition (Shen et al., 2009).

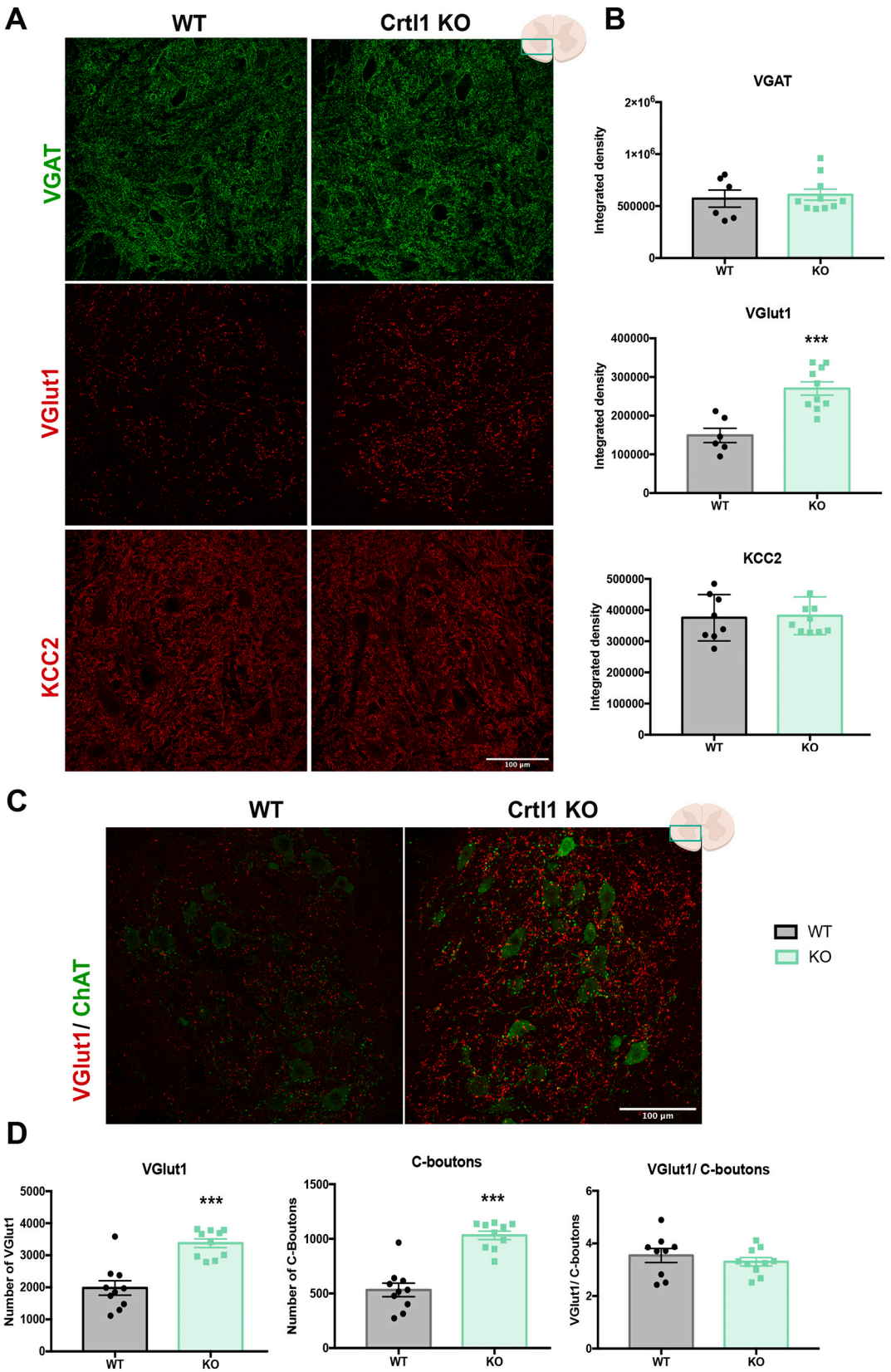

Fig. 8. ***Crtl1*** **KO mice exhibited a general increase in excitatory synapses around lumbar motoneurons**. A. Confocal images representing synapses around lumbar motoneurons (VGAT and VGlut1) and the KCC2 transporter anchored in motoneurons membrane. B. Quantification of the integrated density of the immunoreactive staining around lumbar motoneurons. C. Confocal images showing the amount of proprioceptive afferents (VGlut1) and C-boutons (ChAT) in *Crtl1* KO and WT mice. D. Quantification of the number of VGlut1 and CHAT-positive dots and their ratio. Scale bar: 100 µm. $N_{total} = 20$ mice. Bar graphs are representing the mean values ± SEM. $^{**}p < 0.01$, $^{***}p < 0.001$ by unpaired t-test. VGlut1: vesicular glutamate transporter 1; VGAT: vesicular GABA transporter; ChAT: choline acetyltransferase; Crtl1: cartilage link protein 1; WT: wild type; KO: knock-out.

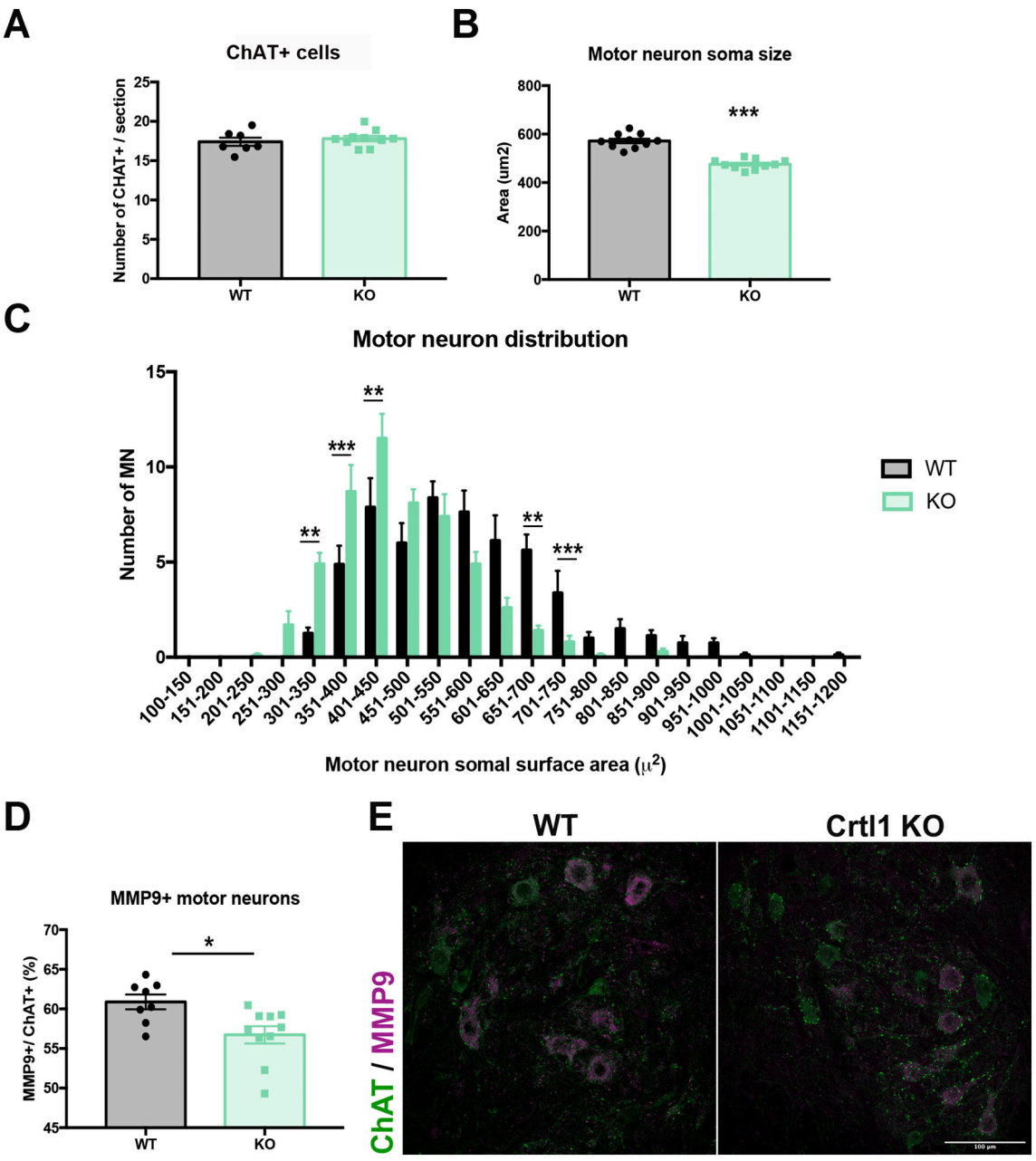

Fig. 9. The lack of link protein 1 modified the properties of lumbar motoneurons. Quantification of the number of ChAT-positive cells/ section of the lumbar spinal cord (A) and the neuronal soma area (B). C. Motoneuron distribution of 55–70 motoneurons/animal based on the neuronal soma surface area. D. Percentage of ChAT-positive cells stained against the MMP9 marker. E. Representative microphotographs of the ventral horn of the lumbar spinal cord in which ChAT-positive (green) and MMP9-positive (purple) are shown. Scale bar: 100 μm. $N_{total} = 20$ mice. Data are representing the mean values ± SEM. *$p < 0.05$, ***$p < 0.001$ by unpaired t-test. **$p < 0.01$, ***$p < 0.001$ by two-way ANOVA (time $F_{21,336} = 47.31$, $p < 0.001$; group $F_{1,16} = 1.012$, $p = 0.329$; interaction $F_{21,336} = 5.684$, $p < 0.001$) followed by post hoc test with Bonferroni correction. ChAT: choline acetyltransferase, MMP9: matrix metalloproteinase 9; Crtl1: cartilage link protein 1; WT: wild type; KO: knock-out. (For interpretation of the references to colour in this figure legend, the reader is referred to the web version of this article.)

This increased synapse formation was also observed in mice lacking different PNN components (Geissler et al., 2013) and after ChABC injection (Pyka et al., 2011). Interestingly, ChABC application modifies both inhibitory and excitatory neurotransmission. The lack of inhibitory inputs in our transgenic mice could be attributed to the buffering role of PNNs conferred by the negative charge of their CSPGs. Both CSPG digestion and PNN reduction around denervated neurons after SCI change the transmembrane Cl- gradient, altering GABAergic neurotransmission (Geissler et al., 2013; Hirono et al., 2018; Sánchez-Ventura et al., 2020). However, *Crtl1* KO mice had CSPGs accumulating around the neuronal soma, whose negative charge can still have functional effects (Glykys et al., 2014). Similarly, the presence of the tenascin-R protein, which regulates GABA release (Saghatelyan et al., 2000), can also contribute to the maintenance of inhibitory synapses in these transgenic animals. Thus, the altered composition of PNNs on *Crtl1* KO mice produce an increased number of excitatory but not inhibitory synapses.

Specifically, we observed and increase of VGlut1-labeled boutons, corresponding to proprioceptive contacts (Alvarez et al., 2004). In fact, PNN breakdown has been associated with altered glutamatergic transmission (Frischknecht et al., 2009). We also observed an increased amount of C-boutons, corresponding to cholinergic interneurons (Witts

et al., 2014). This finding is quite interesting since prior work has suggested that cholinergic and proprioceptive inputs compete for contact spinal MNs, dependent on neural activity. Thus, increased activity in proprioceptive terminals should correlate with fewer cholinergic inputs and vice versa (Jiang et al., 2016). Our findings suggest that this synaptic competition was absent in *Crlt1* KO mice, where both VGlut1 and C-bouton inputs were increased, probably because MNs with altered PNNs have more synaptic space available. Nevertheless, these newly formed synapses might not be functional (Geissler et al., 2013).

The increase in excitatory synapses found in the ventral and dorsal horn can foster a more excitable milieu in the developmental spinal cord, that can affect MN maturation and motor circuitry function. *Crtl1* KO mice showed an increased number of small MNs and a reduction of larger ones. The increased excitability found in the spinal cord of KO mice may affect the physiological properties of α-MNs during development, directing the maturation of MNs into a more excitable phenotype, compatible with smaller MNs (de Martínez-Silva et al., 2018). In fact, fast and slow MNs have different excitability, and this can already be distinguished in the neonatal stage based on their firing pattern (Manuel and Zytnicki, 2019). Since PNNs can affect this firing pattern, and aberrant PNNs increase the membrane capacitance leading to excitable changes (Tewari et al., 2018), it is plausible that altered PNNs generate a slow MN-like firing pattern that increases the percentage of MNs maturing towards a slower profile. In fact, the role of PNNs in neural maturation was already described in parvalbumin-positive cells (Sugiyama et al., 2008; Beurdeley et al., 2012). Overall, a correct PNN composition might be crucial for the function and identity of MNs, and their disorganization can affect the role and the connectivity of these neurons.

These changes in the properties of lumbar MNs have an impact on neuromuscular function. Indeed, the loss of fast MNs, which tend to innervate more and larger muscle fibers (Manuel and Zytnicki, 2019), can explain the decreased number of muscle fibers and the reduced weight of the tibialis anterior muscle. To compensate the loss of fast MNs, slow MNs would comparatively innervate more fibers than WT mice generating bigger amplitudes and thus, becoming larger than the ones from WT mice (Suppl Fig. 6). However, these small changes did not have a functional repercussion on the muscle force assessment.

4.3. The disruption of spinal circuits leads to motor impairment

By electrophysiological tests, we evaluated monosynaptic and polysynaptic reflexes and we observed an increased excitability in the spinal circuits of *Crtl1* KO mice. We also detected a reduction in both initial and final latencies of M wave in *Crtl1* KO mice compared to WT. However, this reduction is unlikely to be related to altered nerve conduction velocity, since the formation of the nodes of Ranvier depends on link protein 2 expression (Bekku et al., 2010). Neurocan reduction could indirectly affect the structure of the node of Ranvier, which is also rich in CSPGs (Bekku and Oohashi, 2011), but we think that these shorter latencies can be easily explained by the reduced size of *Crtl1* KO mice.

Moreover, *Crtl1* KO mice presented hypoactivity and impaired motor function in the different functional tests performed. The hypoactivity observed could be explained by fewer fast MNs, which innervate rapidly contracting motor units (Olson and Swett Jr., 1969). The motor impairment was confirmed in the rotarod and pole tests, after observing that *Crtl1* KO mice could not reach the maximum velocity obtained by WT, lasted a shorter time in the rotarod and needed more time to descend the pole. These results together with the gait abnormalities observed in the DigiGait analysis suggested impaired motor coordination in mice with altered PNNs. Similar functional outcomes were reported by *Freitag* et al. in animals with altered PNNs (Freitag et al., 2003). *Crtl1* KO mice also present altered motor learning, assessed by the adapted rotarod. Learning and memory processes have been studied in the brain of animals with altered PNNs (Montag-Sallaz and Montag, 2003) or after ChABC administration (Hylin et al., 2013; Tsien, 2013). In our study, *Crtl1* KO mice exhibited impaired memory consolidation, but improved ability to recognize a new object, as previously described (Romberg et al., 2013). However, this is the first time that motor learning has been assessed in the context of spinal PNNs.

Overall, the present work demonstrates the involvement of PNNs in motor function through properly wiring spinal circuits and determining the identity of lumbar MNs. Nevertheless, alteration of PNNs located in brain regions related to motor control, as well as the skeletal abnormalities described in these mice (Czipri et al., 2003), can contribute to this motor impairment.

4.4. Aberrant PNNs increase sprouting after spinal cord injury

The role of PNNs in restricting plasticity has been known for decades (Pizzorusso, 2002). In fact, ChABC application has been widely used to promote axon growth. When it is applied in a denervated sensory nucleus of the brainstem after a cervical SCI, an increased collateral sprouting is observed (Massey et al., 2006). Increased plasticity was also observed in our *Crtl1* KO mice, shown by enhanced sprouting of spared contralateral axons after injuring the corticospinal tract. Therefore, alterations of PNNs generate a growth permissive environment for axons to sprout after injury. However, the application of ChABC has a stronger impact on the sprouting of spared axons compared to our *Crtl1* KO mice, based on the percentage of sprouting of contralateral axons below the injury (Starkey et al., 2012). This can be due to the incomplete loss of CSPGs around *Crtl1* KO mice's neurons, that inhibits neural regeneration (Shen et al., 2009). Moreover, ChABC acts on all CSPGs in the CNS, although only 2% are in PNNs (Fawcett, 2015), facilitating a more plastic milieu and hindering the distinction of the effects of modifying PNNs or the whole ECM. Hence, despite aberrant PNNs lead to detrimental effects at the locomotion level, they are beneficial promoting regeneration after a SCI. Thus, any therapeutical modulation of spinal PNNs must consider the balance between synaptic integrity and plasticity.

5. Conclusion

The present study demonstrates that aberrant PNNs enhance excitatory synapses and change the physiological properties of lumbar MNs, overall altering spinal circuits and producing motor impairment. This disorganization generates a permissive scenario for contralateral axons to sprout after SCI. Thus, new strategies to promote regeneration after injury require a more refined PNN modulation to strike an accurate balance between promoting plasticity and maintaining the beneficial properties of PNNs. In conclusion, PNNs' malleability makes them a potential therapeutic target to treat neural disorders in which plasticity and stability are key elements to consider.

Supplementary data to this article can be found online at https://doi.org/10.1016/j.expneurol.2022.114220.

Author contribution

JSV contributed to the design of the experiments, performed the experiments, analyzed the data, and wrote the original draft of the manuscript. CC and JH contribute to the design and analysis of the behavior experiments and reviewed and edited the manuscript. CP performed some of the surgical procedures and reviewed and edited the manuscript. XN supervised some of the electrophysiological tests and analysis of data and reviewed and edited the manuscript. KF and ATE contributed to the design of the experiments, analysis of the data and reviewed and edited the manuscript. EU acquired the funding, designed the study, contributed to the analysis of the data, and reviewed and edited the manuscript.

Declaration of Competing Interest

Authors declare no conflict of interest.

Data availability

Data will be made available on request.

Acknowledgments

This work was funded by the Fundació La Marató-TV3 (TV3-201736-30-31) and by funds from CIBERNED and TERCEL networks, co-funded by European Union (ERDF/ESF, "Investing in your future"). JSV holds a predoctoral fellowship of the AGAUR, Secretaria d'Universitats i Recerca del Departament d'Empresa i Coneixement de la Generalitat de Catalunya, cofunded by European Social Funds. CC and JH acknowledge the support of PIF UAB fellowship, and of Ministerio de Economía y Competitividad y Fondo Europeo de Desarrollo Regional (RTI2018-101105-B-I00), respectively.

We thank Dr. Pizzorusso for the donation of *Crtl1* KO mice. We also appreciate the technical help of Mònica Espejo, Jessica Jaramillo and Neus Hernández, and the Servei de Microscopia de la Universitat Autònoma de Barcelona. We also thank the help of Dr. Joost Verhaagen and Dra Daniela Carulli for technical support on Sem3A staining and analysis. Finally, we thank Dr. Francesc Jiménez-Altayó and Dr. Emma Puighermanal for letting us use their rotarod and pole test, respectively (Universitat Autònoma de Barcelona) and Dr. Michael A. Lane for the revision of the manuscript.

References

Alvarez, F.J., Villalba, R.M., Zerda, R., Schneider, S.P., 2004. Vesicular glutamate transporters in the spinal cord, with special reference to sensory primary afferent synapses. J. Comp. Neurol. 472, 257–280.

Arbat-Plana, A., Torres-Espín, A., Navarro, X., Udina, E., 2015. Activity dependent therapies modulate the spinal changes that motoneurons suffer after a peripheral nerve injury. Exp. Neurol. 263, 293–305.

Barritt, A.W., Davies, M., Marchand, F., Hartley, R., Grist, J., Yip, P., McMahon, S.B., Bradbury, E.J., 2006. Chondroitinase ABC promotes sprouting of intact and injured spinal systems after spinal cord injury. J. Neurosci. 26, 10856–10867.

Bekku, Y., Oohashi, T., 2011. Neurocan contributes to the molecular heterogeneity of the perinodal ECM. Arch. Histol. Cytol. 73, 95–102.

Bekku, Y., Vargová, L., Goto, Y., Vorísek, I., Dmytrenko, L., Narasaki, M., Ohtsuka, A., Fässler, R., Ninomiya, Y., Syková, E., Oohashi, T., 2010. Bral1: Its role in diffusion barrier formation and conduction velocity in the CNS. J. Neurosci. 30, 3113–3123.

Berardi, N., Pizzorusso, T., Maffei, L., 2000. Critical periods during sensory development. Curr. Opin. Neurobiol. 10, 138–145.

Beurdeley, M., Spatazza, J., Lee, H.H.C., Sugiyama, S., Bernard, C., Di Nardo, A.A., Hensch, T.K., Prochiantz, A., 2012. Otx2 binding to perineuronal nets persistently regulates plasticity in the mature visual cortex. J. Neurosci. 32, 9429–9437.

Bevins, R.A., Besheer, J., 2006. Object recognition in rats and mice: a one-trial non-matching-to-sample learning task to study "recognition memory". Nat. Protoc. 1, 1306–1311.

Boulenguez, P., Liabeuf, S., Bos, R., Bras, H., Jean-Xavier, C., Brocard, C., Stil, A., Darbon, P., Cattaert, D., Delpire, E., Marsala, M., Vinay, L., 2010. Down-regulation of the potassium-chloride cotransporter KCC2 contributes to spasticity after spinal cord injury. Nat. Med. 16, 302–307.

Bradbury, E.J., Moon, L.D.F., Popat, R.J., King, V.R., Bennett, G.S., Patel, P.N., Fawcett, J.W., McMahon, S.B., 2002. Chondroitinase ABC promotes functional recovery after spinal cord injury. Nature 416, 636–640.

Brückner, G., Brauer, K., Härtig, W., Wolff, J.R., Rickmann, M.J., Derouiche, A., Delpech, B., Girard, N., Oertel, W.H., Reichenbach, A., 1993. Perineuronal nets provide a polyanionic, glia-associated form of microenvironment around certain neurons in many parts of the rat brain. Glia 8, 183–200.

Carulli, D., Pizzorusso, T., Kwok, J.C.F., Putignano, E., Poli, A., Forostyak, S., Andrews, M.R., Deepa, S.S., Glant, T.T., Fawcett, J.W., 2010. Animals lacking link protein have attenuated perineuronal nets and persistent plasticity. Brain 133, 2331–2347.

Carulli, D., Broersen, R., de Winter, F., Muir, E.M., Meškovic, M., de Waal, M., de Vries, S., Boele, H.J., Canto, C.B., de Zeeuw, C.I., Verhaagen, J., 2020. Cerebellar plasticity and associative memories are controlled by perineuronal nets. Proc. Natl. Acad. Sci. U. S. A. 117, 6855–6865.

Czipri, M., Otto, J.M., Cs-Szabó, G., Kamath, R.V., Vermes, C., Firneisz, G., Kolman, K.J., Watanabe, H., Li, Y., Roughley, P.J., Yamada, Y., Olsen, B.R., Glant, T.T., 2003. Genetic rescue of chondrodysplasia and the perinatal lethal effect of cartilage link protein deficiency. J. Biol. Chem. 278, 39214–39223.

de Martínez-Silva, M.L., Imhoff-Manuel, R.D., Sharma, A., Heckman, C.J., Shneider, N.A., Roselli, F., Zytnicki, D., Manuel, M., 2018. Hypoexcitability precedes denervation in the large fast-contracting motor units in two unrelated mouse models of ALS. Elife 7, 1–26.

Dick, G., Liktan, C., Alves, J.N., Ehlert, E.M.E., Miller, G.M., Hsieh-Wilson, L.C., Sugahara, K., Oosterhof, A., van Kuppevelt, T.H., Verhaagen, J., Fawcett, J.W., Kwok, J.C.F., 2013. Semaphorin 3A binds to the perineuronal nets via chondroitin sulfate type E motifs in rodent brains. J. Biol. Chem. 288, 27384–27395.

Dityatev, A., Brückner, G., Dityateva, G., Grosche, J., Kleene, R., Schachner, M., 2007. Activity-dependent formation and functions of chondroitin sulfate-rich extracellular matrix of perineuronal nets. Dev. Neurobiol. 67, 570–588.

Faist, M., Mazevet, D., Dietz, V., Pierrot-Deseilligny, E., 1994. A quantitative assessment of presynaptic inhibition of la afferents in spastics: differences in hemiplegics and paraplegics. Brain 117, 1449–1455.

Fawcett, J.W., 2015. The Extracellular Matrix in Plasticity and Regeneration after CNS Injury and Neurodegenerative Disease. Elsevier B.V.

Fawcett, J.W., Oohashi, T., Pizzorusso, T., 2019. The roles of perineuronal nets and the perinodal extracellular matrix in neuronal function. Nat. Rev. Neurosci. 20, 451–465.

Foscarin, S., Ponchione, D., Pajaj, E., Leto, K., Gawlak, M., Wilczynski, G.M., Rossi, F., Carulli, D., 2011. Experience-dependent plasticity and modulation of growth regulatory molecules at central synapses. PLoS One 6.

Freitag, S., Schachner, M., Morellini, F., 2003. Behavioral alterations in mice deficient for the extracellular matrix glycoprotein tenascin-R. Behav. Brain Res. 145, 189–207.

Friese, A., Kaltschmidt, J.A., Ladle, D.R., Sigrist, M., Jessell, T.M., Arbera, S., 2009. Gamma and alpha motor neurons distinguished by expression of transcription factor Err3. Proc. Natl. Acad. Sci. U. S. A. 106, 13588–13593.

Frischknecht, R., Heine, M., Perrais, D., Seidenbecher, C.I., Choquet, D., Gundelfinger, E. D., 2009. Brain extracellular matrix affects AMPA receptor lateral mobility and short-term synaptic plasticity. Nat. Neurosci. 12, 897–904.

García-Alías, G., Barkhuysen, S., Buckle, M., Fawcett, J.W., 2009. Chondroitinase ABC treatment opens a window of opportunity for task-specific rehabilitation. Nat. Neurosci. 12, 1145–1151.

Geissler, M., Gottschling, C., Aguado, A., Rauch, U., Wetzel, C.H., Hatt, H., Faissner, A., 2013. Primary hippocampal neurons, which lack four crucial extracellular matrix molecules, display abnormalities of synaptic structure and function and severe deficits in perineuronal net formation. J. Neurosci. 33, 7742–7755.

Glykys, J., Dzhala, V., Egawa, K., Balena, T., Saponjian, Y., Kuchibhotla, K.V., Bacskai, B. J., Kahle, K.T., Zeuthen, T., Staley, K.J., 2014. Local impermeant anions establish the neuronal chloride concentration. Science 343, 670–675 (1979).

Hirono, M., Watanabe, S., Karube, F., Fujiyama, F., Kawahara, S., Nagao, S., Yanagawa, Y., Misonou, H., 2018. Perineuronal nets in the deep cerebellar nuclei regulate GABAergic transmission and delay eyeblink conditioning. J. Neurosci. 38, 6130–6144.

Ho, S.M., Waite, P.M.E., 2002. Effects of different anesthetics on the paired-pulse depression of the H reflex in adult rat. Exp. Neurol. 177, 494–502.

Hylin, M.J., Orsi, S.A., Moore, A.N., Dash, P.K., 2013. Disruption of the perineuronal net in the hippocampus or medial prefrontal cortex impairs fear conditioning. Learn. Mem. 20, 267–273.

Irvine, S.F., Kwok, J.C.F., 2018. Perineuronal nets in spinal motoneurones: chondroitin sulphate proteoglycan around alpha motoneurones. Int. J. Mol. Sci. 19.

Jiang, Y.-Q., Zaaimi, B., Martin, J.H., 2016. Competition with primary sensory afferents drives remodeling of corticospinal axons in mature spinal motor circuits. J. Neurosci. 36, 193–203.

Kaplan, A., Spiller, K.J., Towne, C., Kannng, K., Choe, G., Geber, A., Akay, T., Aebischer, P., Henderson, C., 2014. Neuronal matrix metalloproteinase-9 is a determinant of selective neurodegeneration. Neuron 81, 333–348.

Kwok, J.C.F., Carulli, D., Fawcett, J.W., 2010. In vitro modeling of perineuronal nets: Hyaluronan synthase and link protein are necessary for their formation and integrity. J. Neurochem. 114, 1447–1459.

Kwok, J.C.F., Dick, G., Wang, D., Fawcett, J.W., 2011. Extracellular matrix and perineuronal nets in CNS repair. Dev. Neurobiol. 71, 1073–1089.

Mancuso, R., Oliván, S., Osta, R., Navarro, X., 2011. Evolution of gait abnormalities in SOD1 G93A transgenic mice. Brain Res. 1406, 65–73.

Manuel, M., Zytnicki, D., 2019. Molecular and electrophysiological properties of mouse motoneuron and motor unit subtypes. Curr. Opin. Physiol. 8, 23–29.

Massey, J.M., Hubscher, C.H., Wagoner, M.R., Decker, J.A., Amps, J., Silver, J., Onifer, S. M., 2006. Chondroitinase ABC digestion of the perineuronal net promotes functional collateral sprouting in the cuneate nucleus after cervical spinal cord injury. J. Neurosci. 26, 4406–4414.

Meyer, O.A., Tilson, H.A., Byrd, W.C., Riley, M.T., 1979. A method for the routine assessment of fore- and hindlimb grip strength of rats and mice. Neurobehav. Toxicol. 1, 233–236.

Montag-Sallaz, M., Montag, D., 2003. Severe cognitive and motor coordination deficits in tenascin-R-deficient mice. Genes Brain Behav. 2, 20–31.

Nadine, G., Pico, C., Andreas, L., Cyril, H., 2009. Perineuronal nets protect fear memories from erasure. Science 325, 1258–1261 (1979).

Ogawa, N., Hirose, Y., Ohara, S., Ono, T., Watanabe, Y., 1985. A simple quantitative bradykinesia test in MPTP-treated mice. Res. Commun. Chem. Pathol. Pharmacol. 50, 435–441.

Olson, C.B., Swett Jr., C.P., 1969. Speed of contraction of skeletal muscle: the effect of hypoactivity and hyperactivity. Arch. Neurol. 20, 263–270.

Pizzorusso, T., 2002. Reactivation of ocular dominance plasticity in the adult visual cortex. Science 298, 1248–1251 (1979).

Pyka, M., Wetzel, C., Aguado, A., Geissler, M., Hatt, H., Faissner, A., 2011. Chondroitin sulfate proteoglycans regulate astrocyte-dependent synaptogenesis and modulate

synaptic activity in primary embryonic hippocampal neurons. Eur. J. Neurosci. 33, 2187–2202.
Romberg, C., Yang, S., Melani, R., Andrews, M.R., Horner, A.E., Spillantini, M.G., Bussey, T.J., Fawcett, J.W., Pizzorusso, T., Saksida, L.M., 2013. Depletion of perineuronal nets enhances recognition memory and long-term depression in the perirhinal cortex. J. Neurosci. 33, 7057–7065.
Saghatelyan, A.K., Gorissen, S., Albert, M., Hertlein, B., Schachner, M., Dityatev, A., 2000. The extracellular matrix molecule tenascin-R and its HNK-1 carbohydrate modulate perisomatic inhibition and long-term potentiation in the CA1 region of the hippocampus. Eur. J. Neurosci. 12, 3331–3342.
Sánchez-Ventura, J., Giménez-Llort, L., Penas, C., Udina, E., 2020. Voluntary wheel running preserves lumbar perineuronal nets, enhances motor functions and prevents hyperreflexia after spinal cord injury. Exp. Neurol. 336.
Seibenhener, M.L., Wooten, M.C., 2015. Use of the open field maze to measure locomotor and anxiety-like behavior in mice. J. Visual. Exp. 1–6.
Shen, Y., Tenney, A.P., Busch, S.A., Horn, K.P., Fernando, X., Liu, K., He, Z., Silver, J., Flanagan, J.G., 2009. PTPσ is a receptor for Chondroitin Sulfate Proteoglycan, an inhibitor of neural regeneration. Science 326, 592–596 (1979).
Shiotsuki, H., Yoshimi, K., Shimo, Y., Funayama, M., Takamatsu, Y., Ikeda, K., Takahashi, R., Kitazawa, S., Hattori, N., 2010. A rotarod test for evaluation of motor skill learning. J. Neurosci. Methods 189, 180–185.
Slaker, M., Churchill, L., Todd, R.P., Blacktop, J.M., Zuloaga, D.G., Raber, J., Darling, R. A., Brown, T.E., Sorg, B.A., 2015. Removal of perineuronal nets in the medial prefrontal cortex impairs the acquisition and reconsolidation of a cocaine-induced conditioned place preference memory. J. Neurosci. 35, 4190–4202.
Smith, C.C., Mauricio, R., Nobre, L., Marsh, B., Wüst, R.C.I., Rossiter, H.B., Ichiyama, R. M., 2015. Differential regulation of perineuronal nets in the brain and spinal cord with exercise training. Brain Res. Bull. 111, 20–26.
Spicer, A.P., Joo, A., Bowling, R.A., 2003. A hyaluronan binding link protein gene family whose members are physically linked adjacent to chrondroitin sulfate proteoglycan core protein genes. The missing links. J. Biol. Chem. 278, 21083–21091.
Starkey, M.L., Bartus, K., Barritt, A.W., Bradbury, E.J., 2012. Chondroitinase ABC promotes compensatory sprouting of the intact corticospinal tract and recovery of forelimb function following unilateral pyramidotomy in adult mice. Eur. J. Neurosci. 36, 3665–3678.
Sugiyama, S., Di Nardo, A.A., Aizawa, S., Matsuo, I., Volovitch, M., Prochiantz, A., Hensch, T.K., 2008. Experience-dependent transfer of Otx2 homeoprotein into the visual cortex activates postnatal plasticity. Cell 134, 508–520.
Suttkus, A., Rohn, S., Weigel, S., Glöckner, P., Arendt, T., Morawski, M., 2014. Aggrecan, link protein and tenascin-R are essential components of the perineuronal net to protect neurons against iron-induced oxidative stress. Cell Death Dis. 5, 1–12.
Tewari, B.P., Chaunsali, L., Campbell, S.L., Patel, D.C., Goode, A.E., Sontheimer, H., 2018. Perineuronal nets decrease membrane capacitance of peritumoral fast spiking interneurons in a model of epilepsy. Nature. Communications 9.
Thompson, F.J., Reier, P.J., Lucas, C.C., Parmer, R., 1992. Altered patterns of reflex excitability subsequent to contusion injury of the rat spinal cord. J. Neurophysiol. 68, 1473–1486.
Tom, V.J., Kadakia, R., Santi, L., Houlé, J.D., 2009. Administration of chondroitinase ABC rostral or caudal to a spinal cord injury site promotes anatomical but not functional plasticity. J. Neurotrauma 26, 2323–2333.
Tsien, R.Y., 2013. Very long-term memories may be stored in the pattern of holes in the perineuronal net. Proc. Natl. Acad. Sci. U. S. A. 110, 12456–12461.
Valero-Cabré, A., Forés, J., Navarro, X., 2004. Reorganization of reflex responses mediated by different afferent sensory fibers after spinal cord transection. J. Neurophysiol. 91, 2838–2848.
Vavrek, R., Pearse, D.D., Fouad, K., 2007. Neuronal populations capable of regeneration following a combined treatment in rats with spinal cord transection. J. Neurotrauma. 24 (10), 1667–1673. https://doi.org/10.1089/neu.2007.0290. PMID: 17970629.
Vo, T., Carulli, D., Ehlert, E.M.E., Kwok, J.C.F., Dick, G., Mecollari, V., Moloney, E.B., Neufeld, G., de Winter, F., Fawcett, J.W., Verhaagen, J., 2013. The chemorepulsive axon guidance protein semaphorin3A is a constituent of perineuronal nets in the adult rodent brain. Mol. Cell. Neurosci. 56, 186–200.
Wang, D., Fawcett, J., 2012. The perineuronal net and the control of cns plasticity. Cell Tissue Res. 349, 147–160.
Wang, D., Ichiyama, R.M., Zhao, R., Andrews, M.R., Fawcett, J.W., 2011. Chondroitinase combined with rehabilitation promotes recovery of forelimb function in rats with chronic spinal cord injury. J. Neurosci. 31, 9332–9344.
Witts, E.C., Zagoraiou, L., Miles, G.B., 2014. Anatomy and function of cholinergic C Bouton inputs to motor neurons. J. Anat. 224, 52–60.